



# Loss of lamin-B1 and defective nuclear morphology are hallmarks of astrocyte senescence in vitro and in the aging human hippocampus

Isadora Matias<sup>1</sup> | Luan Pereira Diniz<sup>1</sup> | Isabella Vivarini Damico<sup>1</sup> | Ana Paula Bergamo Araujo<sup>1</sup> | Laís da Silva Neves<sup>1</sup> | Gabriele Vargas<sup>1</sup> | Renata E. P. Leite<sup>2,3</sup> | Cláudia K. Suemoto<sup>2,3</sup> | Ricardo Nitrini<sup>2</sup> | Wilson Jacob-Filho<sup>2,3</sup> | Lea T. Grinberg<sup>2,4,5</sup> | Elly M. Hol<sup>6</sup> | Jinte Middeldorp<sup>6,7</sup> | Flávia Carvalho Alcantara Gomes<sup>1</sup>

<sup>1</sup>Institute of Biomedical Sciences, Federal University of Rio de Janeiro, Rio de Janeiro, Brazil

<sup>2</sup>Brazilian Aging Brain Study Group, University of São Paulo Medical School, São Paulo, Brazil

<sup>3</sup>Division of Geriatrics, University of São Paulo Medical School, São Paulo, Brazil

<sup>4</sup>Department of Neurology, Memory and Aging Center, University of California San Francisco, San Francisco, California, USA

<sup>5</sup>Department of Pathology, University of California San Francisco, San Francisco, California, USA

<sup>6</sup>Department of Translational Neuroscience, University Medical Center Utrecht Brain Center, Utrecht University, Utrecht, The Netherlands

<sup>7</sup>Department of Immunobiology, Biomedical Primate Research Center, Rijswijk, The Netherlands

## Correspondence

Flávia Carvalho Alcantara Gomes and Isadora Matias, Institute of Biomedical Sciences, Federal University of Rio de Janeiro, Centro de Ciências da Saúde, Bloco F, Ilha do Fundão, 21941-902 – Rio de Janeiro, RJ, Brazil.  
Emails: fgomes@icb.ufrj.br (FCAG); isadora.biomed@gmail.com (IM)

## Funding information

Instituto Nacional de Neurociência Translacional; U.S. Department of Health and Human Services; Ministério da Saúde, Departamento de Ciência e Tecnologia; Fiocruz-MS-Servier Award; ZonMW Memorabel and Alzheimer Nederland; Conselho Nacional de Desenvolvimento Científico e Tecnológico; Coordenação de Aperfeiçoamento de Pessoal de Nível Superior; Fundação Carlos Chagas Filho de Amparo à Pesquisa do Estado do Rio de Janeiro; Fundação de Amparo à Pesquisa do Estado de São Paulo

## Abstract

The increase in senescent cells in tissues, including the brain, is a general feature of normal aging and age-related pathologies. Senescent cells exhibit a specific phenotype, which includes an altered nuclear morphology and transcriptomic changes. Astrocytes undergo senescence in vitro and in age-associated neurodegenerative diseases, but little is known about whether this process also occurs in physiological aging, as well as its functional implication. Here, we investigated astrocyte senescence in vitro, in old mouse brains, and in post-mortem human brain tissue of elderly. We identified a significant loss of lamin-B1, a major component of the nuclear lamina, as a hallmark of senescent astrocytes. We showed a severe reduction of lamin-B1 in the dentate gyrus of aged mice, including in hippocampal astrocytes, and in the granular cell layer of the hippocampus of post-mortem human tissue from non-demented elderly. The lamin-B1 reduction was associated with nuclear deformations, represented by an increased incidence of invaginated nuclei and loss of nuclear circularity in senescent astrocytes in vitro and in the aging human hippocampus. We

**Abbreviations:** 53BP1, p53-binding protein 1; ACM, astrocyte conditioned medium; AD, Alzheimer's disease; Ara C, cytosine arabinoside; BSA, bovine serum albumin; CNS, central nervous system; DHE, dihydroethidium; DIV, days in vitro; DMEM, Dulbecco's minimum essential medium; FBS, fetal bovine serum; FTD, frontotemporal dementia; GAPDH, glyceraldehyde 3-phosphate dehydrogenase; GFAP, glial fibrillary acidic protein; iNOS, inducible nitric oxide synthase; MMP3, metalloproteinase 3; NO, nitric oxide; NO<sub>2</sub><sup>-</sup>, nitrite; PBS, phosphate-buffered saline; PD, Parkinson's disease; SASP, senescence-associated secretory phenotype; SA-β-Gal, senescence-associated β-galactosidase activity; TGF-β1, transforming growth factor-β1.

This is an open access article under the terms of the Creative Commons Attribution License, which permits use, distribution and reproduction in any medium, provided the original work is properly cited.

© 2021 The Authors. *Aging Cell* published by Anatomical Society and John Wiley & Sons Ltd.



also found differences in lamin-B1 levels and astrocyte nuclear morphology between the granular cell layer and polymorphic layer in the elderly human hippocampus, suggesting an intra-regional-dependent aging response of human astrocytes. Moreover, we described senescence-associated impaired neurogenic and synaptogenic capacity of mouse astrocytes. Our findings show that reduction of lamin-B1 is a conserved feature of hippocampal cells aging, including astrocytes, and shed light on significant defects in nuclear lamina structure which may contribute to astrocyte dysfunctions during aging.

**KEYWORDS**

aging, astrocyte, human and mouse hippocampus, lamin-B1, senescence, synapse

## 1 | INTRODUCTION

Aging is characterized by a progressive change in the physiology of brain cells that may contribute to cognitive deficits, leading ultimately to dementia and impairment of quality of life. The unique complexity of the human brain, as well as the increasing longevity of humans, represents additional challenges to prevent and postpone aging effects.

It is estimated that by 2050 the number of people aged 60 and older is double from now, reaching nearly 2.1 billion worldwide (Nations, 2017). In this context, a substantial increase in the incidence of age-associated diseases, such as cancer, diabetes, and neurodegenerative diseases, is expected for the next few years (Hou et al., 2019). However, the mechanisms underlying the transition from a healthy fully functional brain to an elderly increasingly dysfunctional brain are not well understood.

Among the causal factors of aging, cellular senescence is an important tumor suppression mechanism, but it also leads to a harmful cellular phenotype which affects tissue homeostasis and regeneration (Campisi, 2005; Lopez-Otin et al., 2013). Several studies have reported age-related accumulation of senescent cells in humans, non-human primates, and rodents (Herbig et al., 2006; Wang et al., 2009; Yousefzadeh et al., 2020). In the aging brain, neural stem cells, neurons, and glial cells display several features of cellular senescence and have been implicated in the pathogenesis of age-related neurodegenerative diseases, such as Alzheimer's disease (AD) and Parkinson's disease (PD; Cohen & Torres, 2019; Martínez-Cué & Rueda, 2020). However, so far little is known about the impact of glial cell senescence on normal brain aging.

Astrocytes form a large and heterogeneous glial cell population in the central nervous system (CNS), playing several vital roles in brain homeostasis and physiology (Verkhatsky & Nedergaard, 2018). In contrast, astrocyte dysfunction has been associated with many brain disorders, such as AD and PD (Diniz et al., 2019; Matias et al., 2019; Osborn et al., 2016), in which senescent astrocytes accumulate and are linked to neurodegeneration and cognitive and motor impairments in mouse models (Bhat et al., 2012; Bussian

et al., 2018; Chinta et al., 2018). Nevertheless, despite the amount of evidence pointing to the involvement of astrocyte senescence in age-related pathologies, the phenotypic and functional changes of senescent astrocytes in the context of physiological brain aging remain to be elucidated. This is at least partially due to the lack of senescence-associated biomarkers for glial cells. Moreover, most of our knowledge of astrocyte biology and brain aging comes from rodent models. A growing number of studies show the unique complexity of human astrocytes (Barbar et al., 2020; Oberheim et al., 2009) and thus it is important to study whether the mechanisms underlying rodent brain aging also apply to the human brain.

The senescent state usually requires a coordinated activation of well-known molecular changes, which identify senescent cells *in vitro* and *in vivo* (Sharpless & Sherr, 2015). Moreover, senescent cells undergo important morphological changes, including altered nuclear size and shape (Mehta et al., 2007), as well as reduced levels of lamin-B1 (Freund et al., 2012).

Lamin-B1, together with the other nuclear lamins, constitute the major components of the nuclear lamina, where they form a dense filamentous meshwork essential for maintaining the structural and functional integrity of the nucleus (de Leeuw et al., 2018). Mutations in lamin genes cause several devastating human diseases, collectively known as laminopathies, among which are premature aging syndromes (Schreiber & Kennedy, 2013). Interestingly, nuclear deformations and reduced levels of B-type lamins are present in post-mortem human brain tissue of AD and frontotemporal dementia (FTD) patients (Frost et al., 2016; Paonessa et al., 2019). Besides, lamin-B1 loss was found specifically within astrocytes in PD brain tissue, suggesting the contribution of senescent astrocytes to PD pathology (Chinta et al., 2018). Still, it remains to be elucidated whether lamin-B1 levels and nuclear morphology are altered in astrocytes during normal brain aging.

Here, we investigated whether lamin-B1 loss and changes in nuclear morphology accompany astrocyte senescence *in vitro* and in the mouse and human aging brain. Altogether, our findings suggest that lamin-B1 loss and defective nuclear morphology are hallmarks of astrocyte senescence *in vitro* and human hippocampal aging.

## 2 | RESULTS

### 2.1 | Age-related loss of lamin-B1 in the mouse hippocampus

Loss of lamin-B1 has been described as a senescence-associated biomarker in some tissues in vivo (Saito et al., 2019; Wang et al., 2017; Yue et al., 2019), although it remains less known whether this also applies to the aged brain. To address this question, we first examined with immunofluorescence the levels of lamin-B1 in the hippocampal dentate gyrus (granular cell layer and molecular layer) of C57Bl/6 mice at 2–3 months and 18–24 months of age. We observed a steady reduction of more than 75% of lamin-B1 intensity in aged mice compared with young ones (Figure 1a–g). Interestingly, in young mice, lamin-B1 intensity was higher at the subgranular zone and in a few cells of the molecular layer (Figure 1c–c'). In contrast, there was a widespread decline of lamin-B1 throughout the molecular and

granular cell layers of the dentate gyrus in aged mice (Figure 1f–f' and Figure S1).

To further address the subcellular decrease of lamin-B1 in the aged hippocampus, we evaluated lamin-B1 staining in glial fibrillary acidic protein (GFAP)+cells in young and aged mice. While we found ~65% of lamin-B1+/GFAP+cells at hippocampal dentate gyrus of young mice, aged mice showed 25% of lamin-B1+/GFAP+cells (Figure 1h–n).

In addition, to confirm the acquisition of the senescent phenotype by aged astrocytes, we analyzed two well-established markers of DNA damage signaling and the senescence-associated secretory phenotype (SASP): p53-binding protein 1 (53BP1) and transforming growth factor beta 1 (TGF- $\beta$ 1), respectively (Di Micco et al., 2021; Salminen et al., 2011). We observed an increased colocalization of 53BP1 in total cell nuclei, as well as in GFAP+cells nuclei, in the hippocampal dentate gyrus of old mice (Figure S2a–d). Similarly, densitometric analysis of TGF- $\beta$ 1 staining revealed a five times increase in

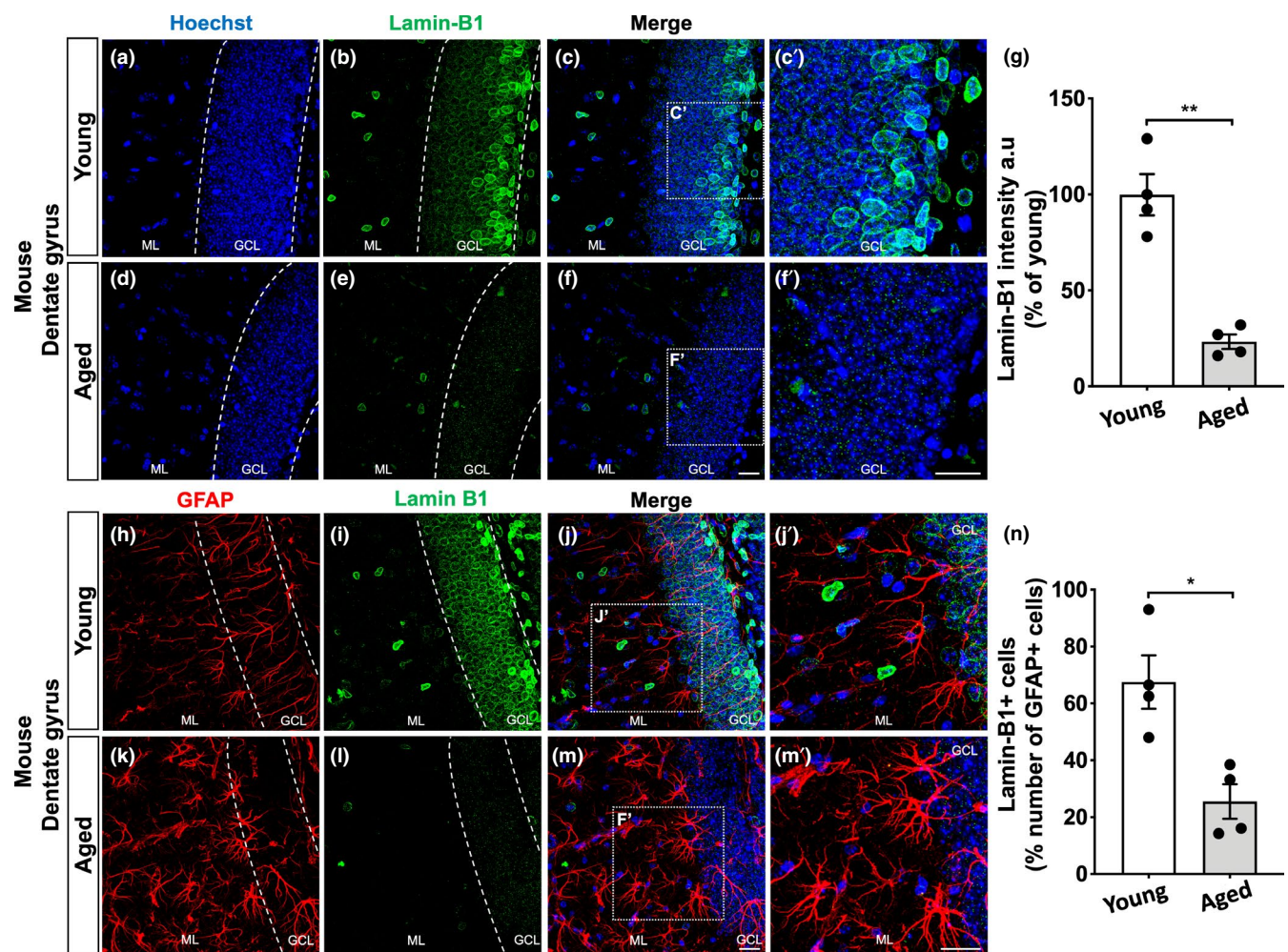


**FIGURE 1** Age-related loss of lamin-B1 in the mouse hippocampus. (a–g) Densitometric analysis of lamin-B1 staining in the mouse hippocampal dentate gyrus, including the molecular layer (ML) and granular cell layer (GCL), revealed a global reduction of lamin-B1 intensity in aged mice compared with young mice ( $p = 0.0033$ ). (h–n) Decreased proportion of lamin-B1 + cells in relation to the total number of GFAP + cells in the dentate gyrus of aged mice compared with young ones ( $p = 0.0126$ ). Significance was determined using unpaired  $t$  test with Welch's correction. Error bars represent  $\pm$ SEM. Individual data points are plotted and represent individual animals ( $n = 4$  animals per experimental group). Scale bars, 20  $\mu$ m



intensity in the molecular layer of the aged dentate gyrus, including a 3.1 times increase in GFAP-positive cells (Figure S2e–h).

Altogether, these results point to an age-related decline of lamin-B1 and upregulation of 53BP1 and TGF- $\beta$ 1 in the mouse hippocampal dentate gyrus, partially due to their regulation in astrocytes, suggesting the acquisition of the senescent phenotype by these cells.

## 2.2 | Senescent astrocytes reveal a distinct phenotype and impaired neurogenic and synaptogenic properties in vitro

To further investigate the molecular and functional changes of aged astrocytes, we first established a new in vitro model for astrocyte senescence by culturing mouse cortical astrocytes for 9–10 days in vitro (DIV, control group) or 30–35 DIV (senescent group) followed by evaluation of several features of cellular senescence (Figure 2a).

We first analyzed the astrocyte cultures for two classical senescence-associated biomarkers: SA- $\beta$ -Gal and the expression of the tumor suppression protein, p16<sup>INK4a</sup> (Sharpless & Sherr, 2015). Accordingly, we observed increased activity of SA- $\beta$ -Gal, based on the optical density of X-Gal staining per experimental condition (Figure 2b–d). Similarly, the percentage of  $\beta$ -Gal+cells was increased by 7.6 times in senescent astrocytes cultures (20.7% of  $\beta$ -Gal+cells) compared with the control group (2.7% of  $\beta$ -Gal+cells) (Figure S3f–h). Additionally, astrocytes cultured for 30–35 DIV showed increased intensity and expression of p16<sup>INK4a</sup> compared with control astrocytes (Figure 2e–h).

Senescent cells are known to express the SASP, linked to increased secretion of several inflammatory mediators, matrix metalloproteinases, and reactive oxygen and nitrogen species (Coppé et al., 2010). In line with this, we observed an upregulation of matrix metalloproteinase 3 (MMP3) and IL-6 mRNA in senescent astrocytes compared with the control group (Figure 2i). Moreover, senescent astrocytes also showed increased levels of reactive oxygen species (Figure 2j–l), as well as higher intensity of inducible nitric oxide synthase (iNOS, Figure 2m–o) and extracellular nitrite (NO<sub>2</sub><sup>-</sup>), a stable metabolite of nitric oxide (NO; Figure 2p). Despite classical features of senescent cells, we did not observe evident morphological changes in astrocytes over time in vitro (Figure S3b–e).

To further investigate the functional implication of the senescent astrocyte phenotype, we have addressed two known properties of astrocytes; induction of neurogenesis and synaptogenesis. To do that, we cultured neural progenitor cells derived from the cerebral cortex of mouse embryos (E14–15) in the presence of astrocyte conditioned medium (ACM) from control or senescent cultures for 48 h (Figure 3a). The number of primary neurites per cell in each experimental condition was quantified based on immunostaining for  $\beta$ -Tubulin III. As expected, ACM from control cultures (ACM-Control) induced neurogenesis, as shown by the increased number of neurites per cell, compared with Dulbecco's minimum essential medium (DMEM; vehicle). Conversely, ACM from senescent cultures

(ACM-Senescent) failed to increase neurogenesis compared to ACM-Control (Figure 3b–e).

Additionally, we treated mature neuronal cultures (12 DIV) with the ACM-Control or ACM-Senescent for 3 h, followed by the analysis of synaptic density, which was based on the immunostaining for pre- (synaptophysin) and post-synaptic (spinophilin) proteins. As previously shown by our group and others, the ACM-Control induces synapse formation in vitro through astrocytes' secretion of synaptogenic factors. In contrast, the ACM-Senescent did not increase synapse formation (in comparison with DMEM), indicating that senescent astrocytes present impaired synaptogenic capacity (Figure 3f–i).

Taken together, these results indicate first, that mouse astrocytes cultured for 30–35 DIV recapitulate key features of the senescent phenotype, and validate their use as an alternative in vitro model for astrocyte senescence. In addition, these results point to a senescence-associated impairment in the neurogenic and synaptogenic properties of astrocytes.

## 2.3 | Nuclear deformations are associated with lamin-B1 loss in cultured senescent astrocytes

Lamin-B1 downregulation has been described as a senescence-associated biomarker in different in vitro models for cellular senescence, including in replicative, oncogene, and DNA damage-induced senescence models (Freund et al., 2012; Limbad et al., 2020). However, less is known about the regulation of lamin-B1 in aged glial cell cultures.

We thus sought to investigate lamin-B1 as an aging biomarker of astrocytes as suggested by hippocampal mouse data by analyzing its levels in control and senescent astrocyte cultures. Immunostaining, Western blotting, and quantitative RT-PCR (qPCR) assays revealed a robust reduction in lamin-B1 intensity (Figure 4a–c), protein level (Figure 4d), and expression (Figure 4e), of approximately 50%, 30%, and 40%, respectively, in senescent astrocytes compared with control cultures.

It has been shown that lamin concentration within the nucleus is essential in regulating nuclear lamina assembly and, therefore, maintaining nuclear structure and function (Guo et al., 2014; Paonessa et al., 2019). In this sense, we investigated the impact of lamin-B1 downregulation in astrocyte nuclear morphology.

We first analyzed the nuclear circularity based on lamin-B1 staining, which has a maximum value of 1 and diminishes as the nuclear shape becomes increasingly convoluted. We observed a significant reduction in nuclear circularity in senescent astrocytes compared with control ones (Figure 4f–j), which had a positive correlation with the reduced intensity of lamin-B1 in senescent cells (Figure 4k).

We next asked whether alterations of the nuclear circularity could be associated with other types of nuclear lamina abnormalities. To do so, we initially performed three-dimensional reconstruction of lamin-B1+ nuclei of astrocytes, based on z-stack fluorescence

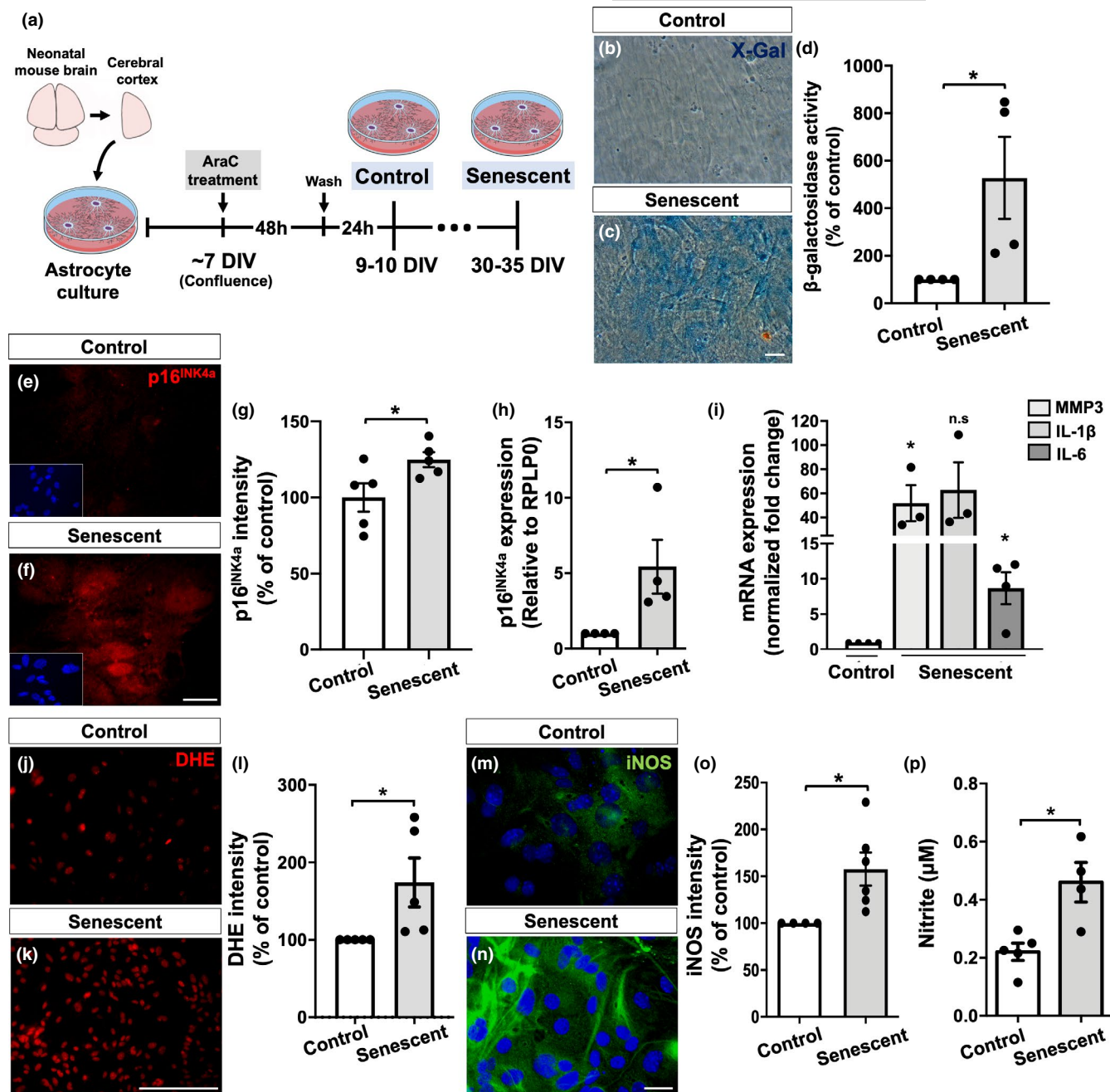


**FIGURE 2** Characterization of a new in vitro model for astrocyte senescence. (a) Primary murine astrocyte cultures were maintained for 9–10 DIV (control group) or 30–35 DIV (senescent group) and analyzed for several senescence-associated biomarkers. (b–d) Astrocytes cultured for 30–35 DIV showed increased SA- $\beta$ -galactosidase activity compared with control cultures ( $p = 0.0481$ ). (e–g) Higher immunostaining for p16<sup>INK4a</sup> in senescent astrocytes compared with control cultures ( $p = 0.0459$ ). (h) Senescent astrocytes showed increased expression of p16<sup>INK4a</sup> ( $p = 0.0471$ ). (i) Expression levels of MMP3 and IL-6 were increased in senescent astrocyte cultures compared with control ones ( $p = 0.0267$  and  $p = 0.0142$ , respectively). (j–l) Increased intensity of DHE labeling (level of ROS) in senescent astrocytes compared with control cultures ( $p = 0.0467$ ). (m–o) Higher immunostaining for iNOS in senescent astrocytes ( $p = 0.0311$ ). (p) Nitrite production was elevated in senescent astrocytes ( $p = 0.0100$ ). Significance was determined using unpaired t test. Error bars represent  $\pm$ SEM. Individual data points are plotted and represent individual cultures ( $n = 3$ –6 cultures per experimental group). Scale bars, 50  $\mu$ m in (c) and 20  $\mu$ m in (f), (k), and (n)

microscopy, to classify the types of nuclear deformations present in control and senescent astrocyte cultures. The nuclear morphological classification was divided into three types: invagination, when nuclei showed one clear lamin-B1 invagination (Figure S4a; Video S1); evagination, when nuclei exhibited one clear lamin-B1 protrusion

from the nuclear lamina (Figure S4b; Video S2); and aberration, when nuclei presented a combination of more than one invagination, evagination or additional nuclear abnormalities (Figure S4c; Video S3). Regular nuclei were considered those without any of these deformations.

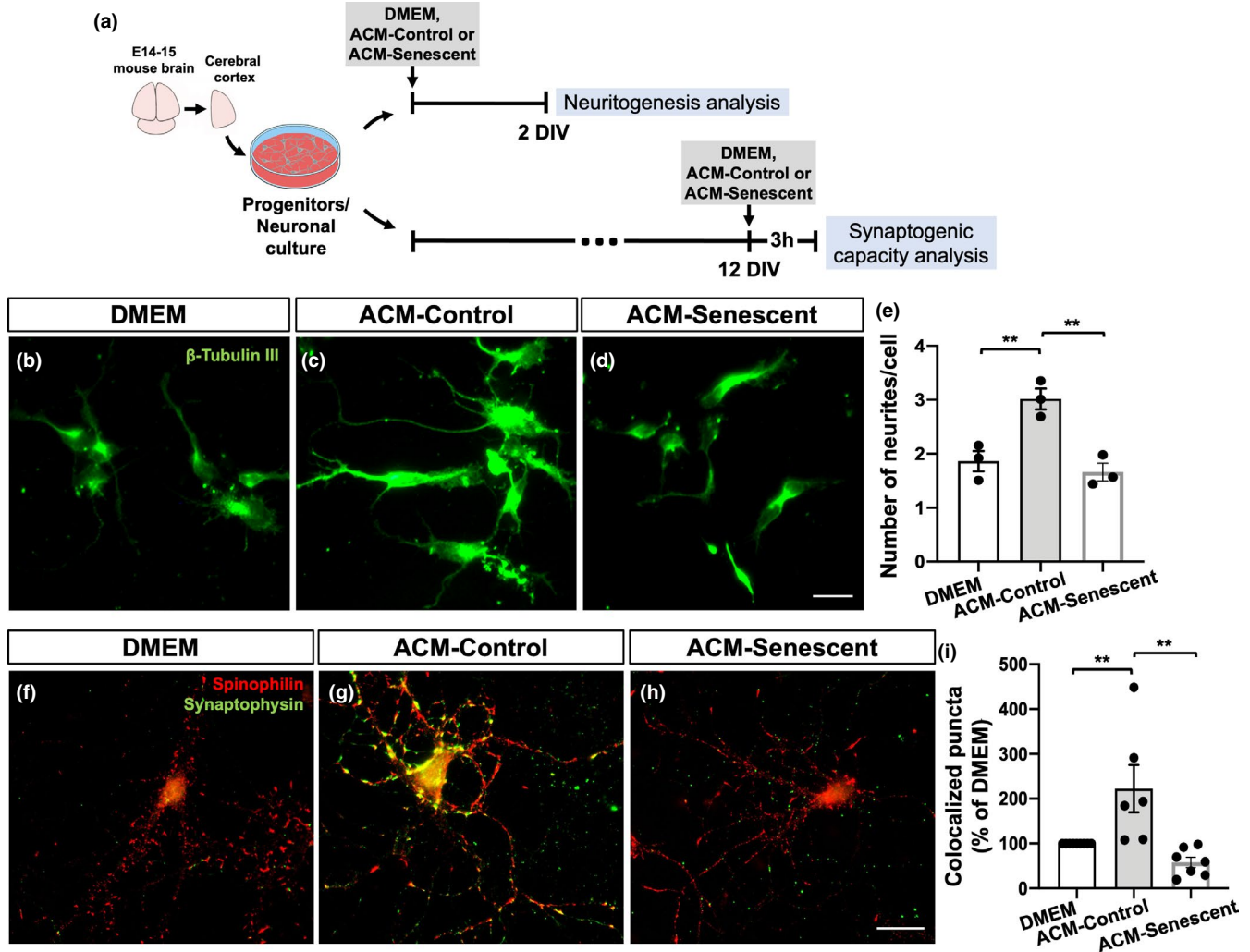


**FIGURE 3** Senescent astrocytes present impaired neuritogenic and synaptogenic properties in vitro. (a) Neural progenitor cell cultures were maintained in DMEM (vehicle), ACM-Control, or ACM-Senescent for 2 DIV. (b–d) The number of primary neurites per cell was quantified based on  $\beta$ -Tubulin III immunostaining. (e) Neural progenitor cells treated with ACM-Control showed increased number of neurites compared with those treated with DMEM ( $p = 0.0097$ ). In contrast, neural progenitors treated with ACM-Senescent exhibited reduced neurite number compared with ACM-Control ( $p = 0.0044$ ). (a, f–h) Mature neurons (12 DIV) were treated with DMEM, ACM-Control, or ACM-Senescent for 3 h, and the number of synapses was quantified based on synaptophysin/spinophilin colocalization puncta. (i) Neurons treated with ACM-Control showed increased percentage of colocalized puncta compared with those treated with DMEM ( $p = 0.0083$ ). Conversely, ACM-Senescent reduced the number of synapses compared with ACM-Control (0.0010). Significance was determined using one-way ANOVA with Tukey's multiple comparisons test. Error bars represent  $\pm$ SEM. Individual data points are plotted and represent individual cultures ( $n = 3$ –9 cultures per experimental condition). Scale bars, 20  $\mu$ m

Therefore, in order to optimize the analysis, we used conventional fluorescence microscopy to image and quantify the number of nuclear deformations in control and senescent astrocyte cultures. We observed a reduced proportion of regular nuclei in senescent astrocyte cultures compared with control astrocytes (Figure 4l–n). This was mainly due to the increased incidence of nuclear invaginations in these cells (Figure 4l–n). The proportion of nuclear evaginations and aberrations was similar between control and senescent astrocytes (Figure 4l–n). Interestingly, the incidence of nuclear invaginations negatively correlated with lamin-B1 intensity in astrocytes (Figure 4o).

Together, these results corroborate previous reports on the lamin-B1 decline in cellular senescence models and provide a new hallmark for astrocyte senescence. Moreover, they strongly indicate

that this process is associated with defects in nuclear morphology, represented by nuclear invaginations and reduced nuclear circularity, which correlate with reduced levels of lamin-B1 in astrocytes.

## 2.4 | Lamin-B1 reduction in the human dentate gyrus upon aging

Whether the mechanisms underlying rodent brain aging apply to the human brain is still a matter of investigation. Thus, we further evaluated whether lamin-B1 downregulation also occurs in the human brain during normal aging. To do so, we gathered post-mortem human hippocampal tissue from two independent brain banks, both

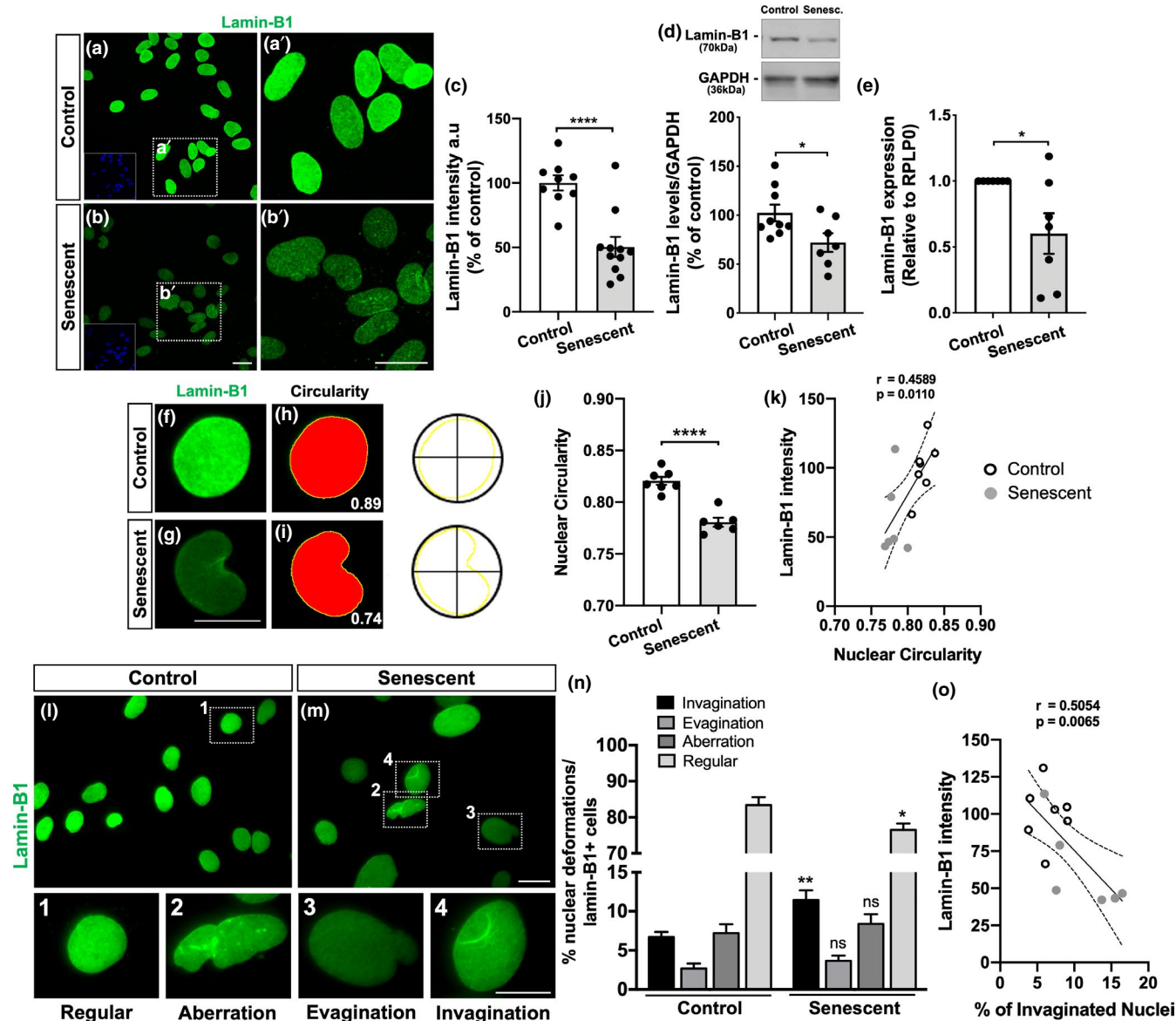


**FIGURE 4** Nuclear deformations are associated with lamin-B1 loss in senescent astrocytes. (a–c) Reduced immunostaining for lamin-B1 in senescent astrocytes compared with the control group ( $p < 0.0001$ ). (d) Lamin-B1 protein levels were diminished in senescent astrocytes in comparison with the control group ( $p = 0.0329$ ). (e) Senescent astrocytes showed decreased expression of lamin-B1 ( $p = 0.0417$ ). (f–i) Nuclear circularity analysis is based on the area and perimeter of the nucleus. Circularity has a maximum value of 1 and diminishes as the nuclear shape becomes increasingly convoluted, as observed in senescent cells (g, i). (j) Senescent astrocytes displayed reduced nuclear circularity compared with the control group ( $p < 0.0001$ ). (k) A positive correlation was observed between lamin-B1 intensity and the nuclear circularity value ( $r = 0.4589$ ;  $p = 0.0110$ ). (l, m) Distinct nuclear morphological profiles were evaluated, such as regular (1), aberration (2), evagination (3), and invagination (4) in control and senescent cultured astrocytes, based on lamin-B1 staining. (n) Senescent astrocyte showed an increased incidence of invaginated nuclei ( $p = 0.0054$ ) and a decreased proportion of regular nuclei ( $p = 0.0263$ ). (o) A negative correlation was observed between lamin-B1 intensity and the incidence of invaginated nuclei ( $r = 0.5054$ ;  $p = 0.0065$ ). Significance was determined using unpaired *t* test with Welch's correction. Linear regression opting to show 95% confidence bands of the best-fit line. Error bars represent  $\pm$ SEM. Individual data points are plotted and represent individual cultures ( $n = 6$ –11 cultures per experimental condition). Control cultures are represented by white dots and senescent cultures by gray dots in (k) and (o). Scale bars, 20  $\mu$ m in (b), (b') and (M); 10  $\mu$ m in (g) and (4)

composed of non-demented controls separated into two age groups: middle-aged and elderly donors. Clinic-pathological information of all donors is present in Table S1.

Densitometric analysis of lamin-B1 immunostaining revealed an overall reduction of approximately 15% in lamin-B1 intensity at the

granular cell layer of the hippocampal dentate gyrus in the elderly compared with middle-aged donors (Figure 5). It is noteworthy that this hippocampal layer is mainly composed of granule neuron cells, and at its inner boundary reside neural stem/progenitor cells and glial cells, especially astrocytes (Casse et al., 2018).



Recent evidence revealed regional heterogeneity upon aging in the mouse and human brain (Boisvert et al., 2018; Soreq et al., 2017). To further investigate lamin-B1 content within the human hippocampus, we also analyzed the polymorphic layer, the innermost layer of the dentate gyrus. Curiously, we did not observe any significant difference in lamin-B1 intensity between middle-aged and elderly donors in this region (Figure S5).

Taken together, these results indicate that human aging is accompanied by a downregulation of lamin-B1 in the granular cell layer of the dentate gyrus. Moreover, they also suggest intra-regional heterogeneity in lamin-B1 regulation within the human hippocampus during aging.

## 2.5 | Human hippocampal neural cells, including astrocytes, undergo nuclear abnormalities upon aging

Recent studies reported that lamin misregulation is associated with defects in neuronal nuclear morphology in age-related neurodegenerative diseases, including FTD and AD (Frost et al., 2016; Paonessa et al., 2019). However, it is still unknown whether these nuclear alterations also occur in neural cells during human brain aging.

Thus, we first analyzed the percentage of regular, evaginated, invaginated, and aberrant lamin-B1+ nuclei in the human hippocampal dentate gyrus from middle-aged and elderly donors. We observed a reduced proportion of regular nuclei at the hippocampal granular cell layer in elderly donors in comparison with middle-aged cases (Figure 6a–c), which was due to increased incidence of nuclear invaginations and aberrations (Figure 6a–c), accounting for a higher proportion of the total nuclear deformations in the elderly hippocampus compared with middle-aged cases (Figure 6d). We did not observe differences in the percentage of nuclear evaginations between

middle-aged and elderly cases at the granular cell layer (Figure 6a–c). Therefore, these results indicate that neural cells, especially granule cells of the dentate gyrus, undergo nuclear invaginations, and aberrations upon human aging.

Human astrocytes have several distinct features from their rodent counterparts including morphological, molecular, and functional properties (Barbar et al., 2020; Oberheim et al., 2009). We then asked whether nuclear abnormalities were also evident in the aged human astrocytes.

As we previously observed, cultured senescent astrocytes presented reduced levels of lamin-B1, which correlated with increased nuclear deformation and decreased nuclear circularity in these cells. Thus, to validate this data, we investigated the nuclear circularity of astrocytes of the granular cell layer from middle-aged and elderly cases. To do so, we used the Hoechst or DAPI nuclear staining, which provided a brighter signal of the nuclei boundaries of GFAP+ astrocytes in post-mortem human tissue. We observed a significant reduction of nuclear circularity in GFAP+ astrocytes from elderly donors compared with middle-aged ones (Figure 6e–g). Additionally, considering the total number of nuclei analyzed at the granular cell layer, we also reported a global reduction of nuclear circularity in elderly donors in comparison with middle-aged donors (Figure 6h).

Since we found age-dependent intra-regional variations in lamin-B1 content between the granular cell layer and the polymorphic layer of the human hippocampus, we asked whether these differences may impact the nuclear morphology of the cells from these two regions during aging. To do so, we analyzed the nuclear morphology at the polymorphic layer based on lamin-B1 staining. Interestingly, we did not observe any significant differences in the proportion of invaginated, evaginated, or aberrant nuclei between middle-aged and elderly cases (Figure

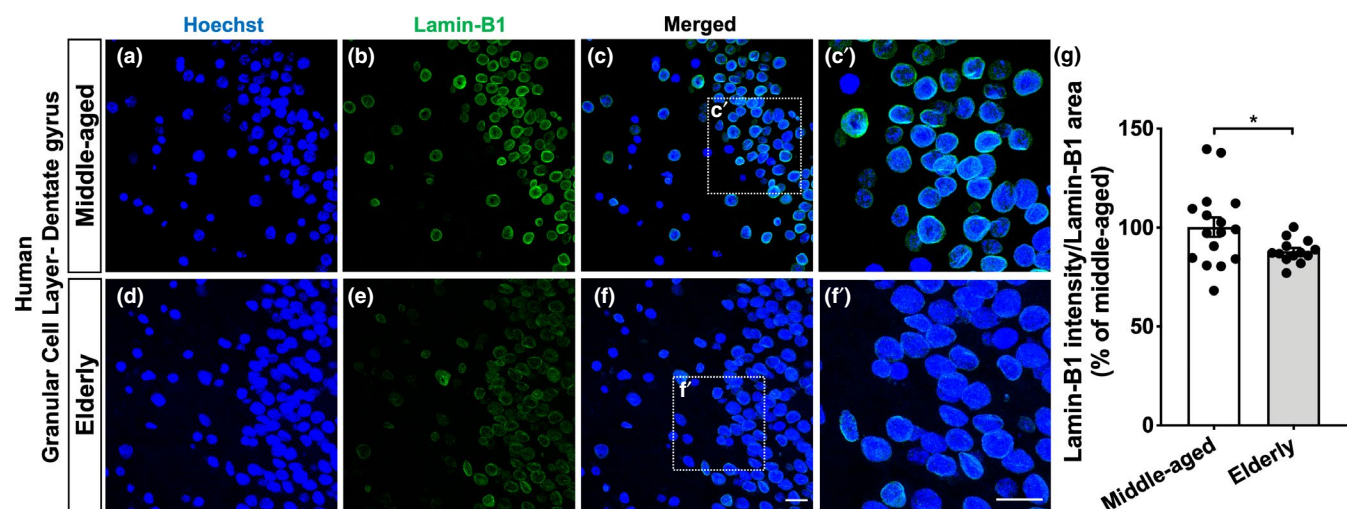


**FIGURE 5** Lamin-B1 reduction in the human dentate gyrus upon aging. (a–g) Densitometric analysis of lamin-B1 staining at the hippocampal granular cell layer from post-mortem human tissue revealed an overall reduction of lamin-B1 intensity in elderly cases compared with middle-aged ones ( $p = 0.0308$ ).  $n = 16$  and  $13$  individuals for middle-aged and elderly groups, respectively. Scale bars,  $20 \mu\text{m}$ . Significance was determined using unpaired  $t$  test with Welch's correction. Error bars represent  $\pm\text{SEM}$ . Individual data points are plotted and represent individual donors



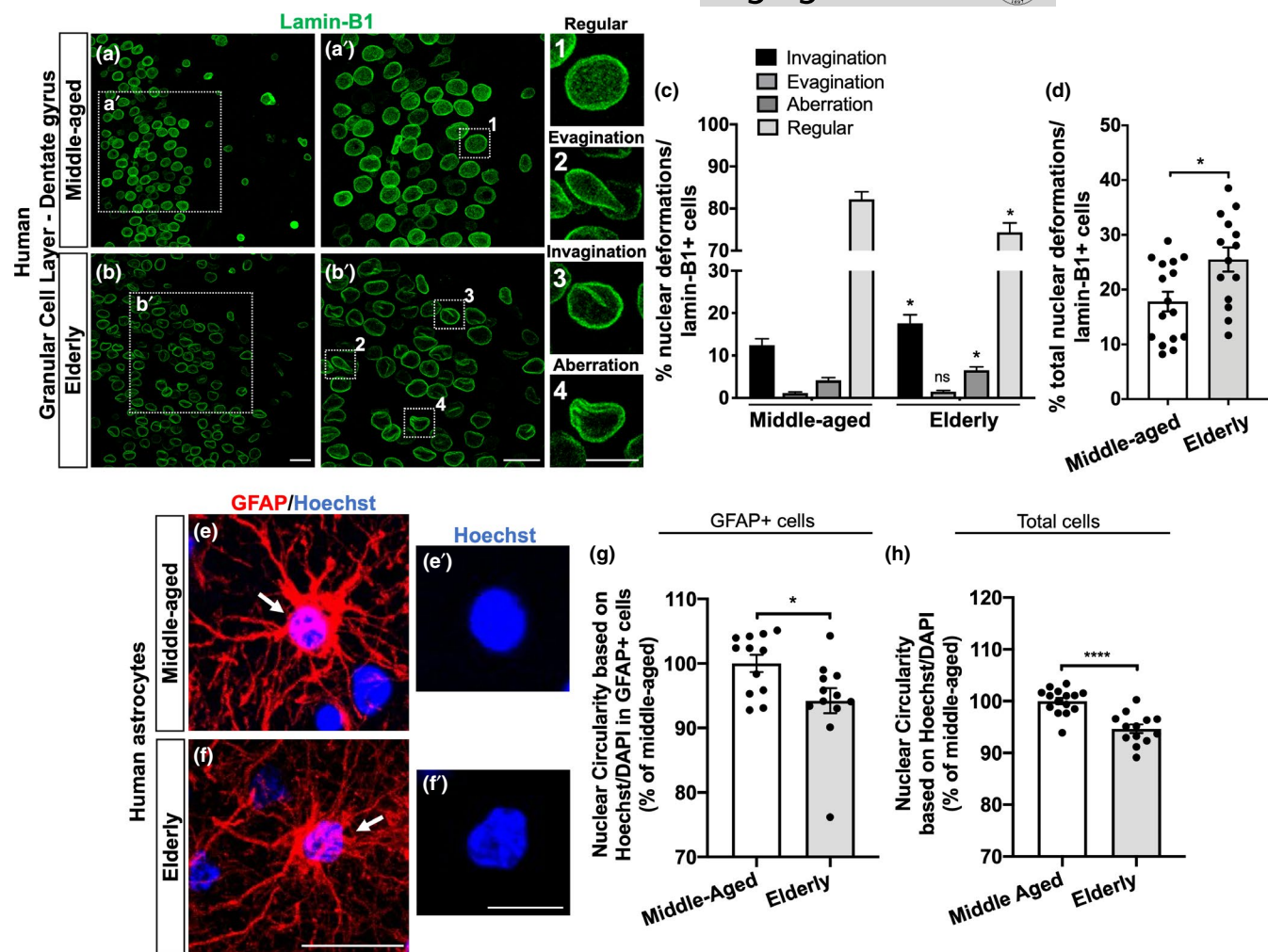


**FIGURE 6** Neural cells, including astrocytes, from the granular cell layer of the human hippocampus undergo nuclear abnormalities upon aging. (a, b) Distinct nuclear morphological profiles were evaluated, such as regular (1), evagination (2), invagination (3), and aberration (4) at the hippocampal granular cell layer in post-mortem human tissue from middle-aged and elderly donors based on lamin-B1 staining. Scale bars, 20  $\mu\text{m}$  in (b) and (b'); 10  $\mu\text{m}$  in (4). (c) Elderly donors exhibited a higher incidence of invaginated ( $p = 0.0494$ ) and aberrant nuclei ( $p = 0.0243$ ), resulting in a decreased proportion of regular nuclei ( $p = 0.0102$ ), compared with the middle-aged group.  $n = 16$  and 14 individuals for middle-aged and elderly groups, respectively. (d) Elderly donors showed an increased proportion of total nuclear deformations (ie, evagination + invagination + aberration) ( $p = 0.0119$ ).  $n = 16$  and 14 individuals for middle-aged and elderly groups, respectively. (e–g) Nuclear circularity was quantified based on Hoechst or DAPI staining in post-mortem human tissue from middle-aged (e–e') and elderly donors (f–f'). Elderly donors presented a reduced nuclear circularity based on the number of GFAP+ cells (g;  $p = 0.0243$ ;  $n = 12$  individuals for both age groups) and on the total number of cells (h;  $p < 0.0001$ ;  $n = 15$  and 13 individuals for middle-aged and elderly groups, respectively). Scale bars, 20  $\mu\text{m}$  in (f) and 10  $\mu\text{m}$  in (f'). Significance was determined using unpaired t test with Welch's correction. Error bars represent  $\pm$  SEM. Individual data points are plotted and represent individual donors

S6a–d). Moreover, in contrast to astrocytes from the granular cell layer, we did not observe a significant reduction of nuclear circularity in GFAP+ astrocytes, nor in the total cells analyzed in the polymorphic layer in elderly donors compared with middle-aged ones (Figure S6e–h).

Taken together, we conclude that human aging is associated with defects in the nuclear morphology of neural cells, including astrocytes, and reduction of the levels of lamin-B1. Those features are heterogeneously distributed in the aging hippocampus. Our data point to a new cellular and molecular marker to the human physiological brain aging and support the emerging concept of regional heterogeneity upon aging.

### 3 | DISCUSSION

In the current study, we have identified that lamin-B1 loss and changes in nuclear morphology are hallmarks of astrocyte senescence in vitro and of neural cells, including astrocytes, in the aging mouse and human hippocampus. By using an in vitro model for astrocyte senescence, we observed that these cells undergo nuclear invaginations and changes in nuclear circularity, which were associated with the loss of lamin-B1. In agreement, these features were also observed in hippocampal astrocytes and granule cells in aged mice and post-mortem human hippocampal tissue from non-demented elderly. In addition, we described that mouse senescent



astrocytes lose their neurotogenic and synaptogenic potential in vitro. Together, our data indicate that astrocytes undergo morphological, molecular, and functional changes during aging and suggest that they may be important targets in understanding the basic mechanisms underlying human hippocampal aging as well as in identifying new age-associated biomarkers.

The hippocampus is critical for cognitive functions and is one of the most vulnerable brain regions to aging and implicated in age-related cognitive decline (Small et al., 2011). Moreover, emerging evidence has pointed to a differential vulnerability of hippocampal subfields in aging and neurodegenerative diseases (Fu et al., 2018; Morrison & Baxter, 2012; Roussarie et al., 2020), being the dentate gyrus particularly affected during normal aging (Morrison & Baxter, 2012; Nadal et al., 2020). Although most of these studies have focused on neuronal populations, recent findings have suggested that major changes in the gene expression profile of glial cells, especially astrocytes, might predict and/or impact the selective vulnerability of brain regions to aging-associated cognitive decline (Boisvert et al., 2018; Clarke et al., 2018; Soreq et al., 2017). Nevertheless, the contribution of astrocyte senescence to aging is far less studied.

The characterization of senescence-associated biomarkers is an important and first step toward understanding the mechanisms underlying senescence itself and its role in the context of aging and age-related diseases. Emerging evidence shows that the loss of lamin-B1 is an important senescence-associated biomarker in several murine and human cell cultures/lines (Freund et al., 2012) and aging tissues, including in photoaged skin (Wang et al., 2017), thymus (Yue et al., 2019), lung (Saito et al., 2019), kidney, and liver (Yousefzadeh et al., 2020). However, relatively less is known about the potential role of lamin-B1 in brain senescence. Here, we demonstrated that lamin-B1 loss is also a hallmark of astrocyte senescence in vitro and described for the first time that its reduction also occurs in hippocampal astrocytes from aged mice, as well as in the hippocampal dentate gyrus from elderly humans. In addition, we reported an overall increase of 53BP1 and TGF- $\beta$ 1 levels in the mouse dentate gyrus, prominently in astrocytes. 53BP1 is one of the mediators of DNA damage checkpoint in response to DNA double-strand breaks (Di Micco et al., 2021). Therefore, it is usually upregulated in aging and cellular senescence models, including in senescent astrocytes induced by ionizing radiation (Turnquist et al., 2019), by the herbicide paraquat (Chinta et al., 2018) and H<sub>2</sub>O<sub>2</sub> treatment (Shang et al., 2020). On the other hand, TGF- $\beta$ 1 is increased with aging and is considered a SASP inducer molecule that can trigger the senescence phenotype in neighboring cells through paracrine signaling (Munoz-Espin & Serrano, 2014; Tominaga & Suzuki, 2019). Thus, our data indicate that the loss of lamin-B1 is accompanied by the acquisition of the senescent phenotype by mouse hippocampal astrocytes upon aging.

We first reported a global reduction of lamin-B1 in the hippocampal dentate gyrus from aged mice, which was partially due to a decreased proportion of hippocampal astrocytes expressing lamin-B1 in this age group. In agreement with our data, a recent study showed age-dependent downregulation of lamin-B1 in adult neural stem/progenitors cells in the mouse hippocampus, which underlies stem

cell aging and negatively impacted adult neurogenesis (Bedrosian et al., 2020). Conversely, restoration of lamin-B1 expression was sufficient to enhance progenitors cells proliferation and neurogenesis in the aged hippocampus (bin Imtiaz et al., 2021).

To further investigate lamin-B1 level in astrocytes, we took advantage of an alternative long-term cell culture model for astrocyte senescence. Astrocytes cultured for 30–35 DIV recapitulated key features of the senescent phenotype, including increased SA- $\beta$ -Gal activity and p16<sup>INK4a</sup> expression, high expression of MMP3, IL-6, and reactive oxygen and nitrogen species, characteristics of SASP. These results corroborate other models previously described to study glial senescence (Bellaver et al., 2017; Bigagli et al., 2016; Pertusa et al., 2007; Souza et al., 2015) and reproduce several glial changes observed in the aging brain, including increased expression of p21, oxidative/nitrosative stress as well as an inflammatory phenotype (Bellaver et al., 2017). Accordingly, astrocytes acutely isolated from the cerebral cortex of aged mice showed a distinct gene expression signature, including an increased inflammatory phenotype (Orre et al., 2014).

It is well-known that astrocytes play several homeostatic functions in the CNS, such as modulating neuronal morphogenesis, synapse formation, and function (Verkhatsky & Nedergaard, 2018). These actions can be triggered by the secretion of neurotrophic and synaptogenic factors, as described by our group and others (Baldwin & Eroglu, 2017; Matias et al., 2019). However, so far, little is known about the functional profile of astrocytes during normal brain aging. Interestingly, hippocampal neurons co-cultured with aged astrocytes showed a decreased excitatory synaptic transmission, due to a reduced pool of readily releasable synaptic vesicles, although the number of synapses was unchanged (Kawano et al., 2012). In our study, we provide the first evidence that senescent astrocytes have impaired neurotogenic and synaptogenic capacity. Neural progenitor cells or mature neurons treated with ACM from senescent astrocytes displayed fewer neurites and synapses, respectively. These results indicate that the content of astrocyte secreted molecules changes upon senescence, suggesting the involvement of these cells in age-related synaptic decline.

Together, these results strongly support the use of long-term cell culture as an in vitro model to investigate the phenotype and function of glial cell senescence. In addition, as shown in the murine hippocampus, we reported reduced levels and expression of lamin-B1 in senescent cultured astrocytes associated with nuclear membrane malformations.

Human astrocytes are distinct from their murine counterparts, morphologically as well as molecularly, pharmacologically, and functionally (Barbar et al., 2020; Oberheim et al., 2009). Limited availability to human post-mortem samples has deeply hampered our understanding of brain aging at the cellular and molecular levels. Whether the mechanisms underlying rodent brain aging apply to the human brain is still a matter of investigation. Here, we took the advantage of analyzing post-mortem human tissue from nondemented elderly and middle-aged donors. We observed reduced intensity of lamin-B1 in hippocampal cells at the granular cell layer



from non-demented elderly donors. This was followed by increased nuclear deformations and a global reduction of nuclear circularity in the elderly hippocampus compared with middle-aged cases. Similarly to senescent mouse astrocytes *in vitro*, we observed a significant reduction of nuclear circularity in GFAP+ astrocytes from elderly donors, suggesting that alteration in nuclear properties might be a conserved characteristic of mice and human astrocyte aging. In agreement with our results, a recent *in vitro* study using X-irradiation induced senescent human astrocytes showed a downregulation of the lamin-B1 gene in these cells, together with higher expression of other classical senescent-associated biomarkers (Limbad et al., 2020).

Curiously, when analyzing lamin-B1 intensity at the polymorphic layer, we did not see a clear reduction of its content, suggesting a region-dependent aging regulation of lamin-B1 levels within the human hippocampus. Recently, it has been shown organ-specific (Schaum et al., 2020) and regional-specific (Boisvert et al., 2018; Pestana et al., 2020; Soreq et al., 2017) molecular signatures during aging. However, whether this intra-regional difference is a predictor of selective vulnerability of the granular cell layer during aging is still unknown.

Taken together, these findings strengthen the hypothesis that lamin-B1 loss, in specific brain areas, is a hallmark associated with cellular senescence, including in astrocytes, in mouse and human hippocampal aging. Although a direct link between lamin-B1 loss with changes in astrocyte phenotype and function has yet to be investigated, lamin-B1 downregulation has been recognized as a key step for the progression of full cellular senescence in other cell types and tissues (Freund et al., 2012; Saito et al., 2019; Shimi et al., 2011), which can, in turn, contribute to tissue degeneration in aging and induce pathological conditions (Saito et al., 2019; Yue et al., 2019). However, whether the lamin-B1 loss is a consequence of the senescent phenotype or a trigger of astrocyte senescence remains to be investigated.

Lamin-B1 is a component of the nuclear lamina and is required for proper organogenesis, cell proliferation, self-maintenance, chromatin structure, nuclear integrity, and gene expression (Ho & Lammerding, 2012). Misregulation of nuclear lamins and abnormalities of the nuclear shape have been widely reported in laminopathies, including premature aging syndromes (Schreiber & Kennedy, 2013), and more recently in *in vivo* models for age-related neurodegenerative diseases. Reduction in lamin-B protein levels and nuclear invaginations have been shown in Tau-transgenic *Drosophila* brains, as well as in AD human brains, events associated with an aberrant cytoskeleton-nucleoskeleton coupling and neuronal death (Frost et al., 2016). Here, we report increased nuclear invagination and abnormal nuclear circularity in senescent astrocytes *in vitro* and in human aged brain. Likewise, a higher incidence of nuclear lamina invaginations is present in FTD human brain tissue and FTD iPSC-derived neurons, resulting in disrupted neuronal nucleocytoplasmic transport *in vitro* (Paonessa et al., 2019).

Astrocyte dysfunctions have been strongly implicated in the pathogenesis of several age-related diseases, although astrocyte

senescence has only recently been fully addressed (Bussian et al., 2018; Chinta et al., 2018; Cohen & Torres, 2019). Recently, it has been shown that senescent astrocytes of PD patients were lamin-B1 deficient, while non-astrocytic neighboring cells retained basal levels of lamin-B1, suggesting that astrocytes may preferentially undergo senescence in PD brain tissue (Chinta et al., 2018). In this sense, this and other studies have shown that depletion of senescent cells, including senescent glial cells, mitigates PD pathology (Chinta et al., 2018), prevents tau-dependent pathology (Bussian et al., 2018), and cognitive deficits in AD mouse models (Zhang et al., 2019).

The fact that loss of lamin-B1 has been reported in age-related neurodegenerative diseases (Chinta et al., 2018; Frost et al., 2016; Paonessa et al., 2019) suggests that this feature may represent an early sign of age-associated brain pathology. Our study demonstrated that lamin-B1 downregulation and nuclear deformations are present in astrocytes (and other neural cells) from post-mortem human tissues from elderly donors, suggesting that astrocytes may play an important role in the mechanisms underlying brain aging.

## 4 | EXPERIMENTAL PROCEDURES

### 4.1 | Animals

Newborn (P0) Swiss mice were used for astrocytes cultures. For *in vivo* experiments, we used male C57Bl/6 mice divided into two age groups: 2–3 months old (young group) and 18–24 months old (aged group). All animals were housed at standard conditions with *ad libitum* access to food and water. Animal handling and experimental procedures were previously approved by the Animal Use Ethics Committee of the Federal University of Rio de Janeiro (CEUA-UFRJ, approval protocol 006/18) and the Central Authority for Scientific Experiments on Animals of the Netherlands (CCD, approval protocol AVD115002016659). Experiments were performed according to Brazilian Guidelines on Care and Use of Animals for Scientific and Teaching Purposes (DBCA) and the Directive of the European Parliament and of the Council of the European Union of 22 September 2010 (2010/63/EU).

### 4.2 | Human post-mortem brain material

Human post-mortem brain material was obtained from two brain banks to increase representation and statistical power: the Netherlands Brain Bank, Amsterdam ([www.brainbank.nl](http://www.brainbank.nl)) (NBB) and the Brain Bank of the Brazilian Aging Brain Study Group, University of São Paulo Medical School (<http://en.gerolab.com.br/>) (BBBABSG). A written informed consent for a brain autopsy and the use of the material and clinical information for research purposes had been obtained by the NBB (project number 1073) and BBBABSG (CAAE number: 30038520.0.0000.5257, approval number 3.986.070). We obtained paraffin-embedded tissue of the hippocampal area from both brain banks. A total of 30 donors were classified into two age



groups: middle-aged (ranged from 50 to 60 years,  $n = 16$ ) and elderly (ranged from 76 to 93 years,  $n = 14$ ). Only non-demented controls were included in the analysis, based on the medical history and pathological scoring. Clinico-pathological information of all donors is present in Table S1.

### 4.3 | Control and senescent astrocyte cultures

Primary cortical astrocyte cultures were derived from newborn Swiss mice as previously described (Matias et al., 2017), and the protocol for senescent astrocyte cultures was adapted from Bigagli et al. (2016). Briefly, cerebral cortices were removed, and the meninges were carefully stripped off. Tissues were maintained in DMEM and nutrient mixture F12 (DMEM/F12, Invitrogen), supplemented with 10% fetal bovine serum (FBS, Invitrogen). Cultures were incubated at 37°C in a humidified 5% CO<sub>2</sub>, 95% air chamber for approximately 7 DIV until confluence. Cultures were separated into two experimental groups: control and senescent astrocyte cultures. After confluence, control astrocyte cultures were treated with cytosine arabinoside (Ara C 10 μM, Sigma) in DMEM/F12 with 10% FBS for 48 h, washed and maintained in DMEM/F12 without FBS for additional 24 h until fixation or protein extraction. In contrast, after the treatment with Ara C, senescent astrocyte cultures were washed and maintained in DMEM/F12 supplemented with 10% FBS for 30–35 DIV, with medium exchange every 2 days. Twenty-four hours before fixation or protein extraction, senescent astrocyte cultures were incubated in DMEM/F12 without FBS.

### 4.4 | Astrocyte-conditioned medium

Control and senescent astrocyte cultures were washed three times to eliminate residual serum and maintained in DMEM/F12 serum-free medium for 24 h. Then, the Astrocyte-conditioned medium (ACM) was collected, centrifuged at 1000 ×  $g$  × 10 min to remove cellular debris, and used immediately or stored in aliquots at –80°C for further use.

### 4.5 | Neuronal culture and treatments

Neuronal cortical cultures were prepared as described previously by our group (Matias et al., 2017). Briefly, the cerebral cortices of embryonic day 14–15 Swiss mice were removed, meninges were carefully removed, neural tissue was dissociated in Neurobasal medium (Invitrogen), and the cells were plated at a density of 75,000 per well of 13 mm diameter onto glass coverslips previously coated with poly-L-lysine (10 μg/ml, Sigma). Cultures were maintained in ACM or Neurobasal medium supplemented with B-27, penicillin, streptomycin, fungizone, L-glutamine, and cytosine arabinoside (0.65 μM, Sigma), at 37°C in a humidified 5% CO<sub>2</sub>, 95% air atmosphere for 2DIV or 12 DIV, respectively. To investigate the effect of the ACM

on neurite formation, neuronal cultures were incubated with DMEM, ACM-Control, or ACM-Senescent for 2 DIV, followed by fixation and immunostaining for β-Tubulin III. To analyze the effect of the ACM on synapse formation, mature neuronal cultures (12 DIV) were incubated with DMEM, ACM-Control, or ACM-Senescent for 3 h, followed by fixation and immunostaining for pre- and post-synaptic markers.

### 4.6 | Immunocytochemistry of astrocyte and neuronal cultures

Astrocyte and neuronal cultures were fixed with 4% PFA in phosphate-buffered saline (PBS; pH 7.4) for 15 min and nonspecific sites were blocked with 3% bovine serum albumin (BSA; Sigma-Aldrich), 5% normal goat serum (Sigma-Aldrich) and 0.2% Triton X-100 diluted in PBS for 1 h, before incubation with the following antibodies: rabbit anti-GFAP (1:1000; DAKO Cytomation), rabbit anti-lamin-B1 (1:1000; Abcam), rabbit anti-p16INK4a (1:100; Proteintech), rabbit anti-iNOS (1:100; Abcam), rabbit anti-Spinophilin (1:500; Abcam), or mouse anti-Synaptophysin (1:1000; Millipore) at 4°C overnight. Subsequently, the cells were thoroughly washed with PBS and incubated with secondary antibodies at room temperature (RT) for 2 h. Secondary antibodies were Alexa Fluor 546-conjugated goat anti-rabbit IgG or goat anti-mouse IgG (1:1000; Invitrogen), or Alexa Fluor 488-conjugated goat anti-rabbit IgG or goat anti-mouse IgG (1:300; Invitrogen). Nuclei were counterstained with DAPI (Sigma-Aldrich), and cells were observed with a TE2000 Nikon microscope.

### 4.7 | Immunohistochemistry of mouse brain tissue

The animals were euthanized by i.p. injection of a lethal dose of sodium pentobarbital (Euthanimal; Alfasan BV, Woerden, The Netherlands) and then transcardially perfused with PBS. Brains were removed and fixed with paraformaldehyde 4% at 4°C for 24 h, then kept in PBS at 4°C. Forty-μm thick sagittal sections were obtained using vibratome (Leica) and subjected to immunohistochemistry. Sections were incubated with blocking buffer composed of 5% normal donkey serum (NDS, Sigma-Aldrich) or 5% normal goat serum (NGS, Sigma-Aldrich), 2% BSA (Sigma-Aldrich), 1% Triton X-100 diluted in PBS for 1 h, before incubation with the following primary antibodies: rabbit anti-lamin-B1 (1:1000; Abcam), mouse anti-GFAP (1:1000; Sigma-Aldrich), mouse anti-GFAP (1:1000; Millipore), rabbit anti-GFAP (1:1000; DakoCytomation), mouse anti-TGF-β1 (1:1000; Abcam), or rabbit anti-53BP1 (1:300; Novus Biologicals) at 4°C for 24 h. The slices were then washed with PBS and incubated with secondary antibodies at RT for 2 h. Secondary antibodies were Alexa Fluor 488-conjugated donkey anti-rabbit IgG (1:1400; Jackson Immuno Research Inc.), Cy3-conjugated donkey anti-mouse IgG (1:1400; Jackson Immuno Research Inc.), Alexa Fluor 594-conjugated goat anti-mouse IgG (1:1000; Molecular Probes), Alexa Fluor 594-conjugated goat anti-rabbit IgG (1:1000; Molecular Probes),



Alexa Fluor 488-conjugated goat anti-rabbit IgG (1:300; Molecular Probes), or Alexa Fluor 488-conjugated goat anti-mouse IgG (1:300; Molecular Probes). Nuclei were counterstained with Hoechst 33528 (1:1000; Thermo Fisher Scientific) and coverslips were mounted in Mowiol (0.1 M Tris, pH 8.5, 25% glycerol, 10% w/v Mowiol 4-88 [Sigma-Aldrich]) or mounting medium (DakoCytomation). Sections were imaged on a confocal microscope Zeiss LSM 880 or Leica TCS SPE.

#### 4.8 | Immunohistochemistry of human paraffin-embedded hippocampal tissue

Immunohistochemistry of human paraffin-embedded tissue was done according to a modified protocol (van Strien et al., 2014). Paraffin sections (7  $\mu$ m thick) were deparaffinized, rehydrated, and washed in distilled water, followed by PBS/0.05% Tween 20 for 30 min. Hereafter, sections were incubated with PBS/0.3% hydrogen peroxide for 10 min, followed by antigen retrieval through exposure heating in a steamer in citrate buffer (10 mM citric acid, 0.05% Tween 20, pH 6.0; 98°C) for 20 min. After cooling down to RT, nonspecific sites were blocked with 5% NDS (Sigma-Aldrich) or 5% normal goat serum (NGS, Sigma-Aldrich), 2% BSA (Sigma-Aldrich), 0.1% Triton X-100 diluted in PBS for 1 h, before incubation with the following primary antibodies: rabbit anti-lamin-B1 (1:1000; Abcam), mouse anti-GFAP (1:1000; Sigma-Aldrich), or mouse anti-GFAP (1:1000; Millipore) at 4°C overnight. The sections were then washed in PBS and incubated with secondary antibodies at RT for 2 h. Secondary antibodies were Alexa Fluor 488-conjugated donkey anti-rabbit IgG (1:1400; Jackson Immuno Research Inc.) Cy3-conjugated donkey anti-mouse IgG (1:1400; Jackson Immuno Research Inc.), Alexa Fluor 594-conjugated goat anti-mouse IgG (1:1000; Molecular Probes), or Alexa Fluor 488-conjugated goat anti-rabbit IgG (1:300; Molecular Probes). Next, sections were washed in PBS and incubated in Sudan Black solution (0.3% Sudan Black in 70% ethanol) for 7 min to quench autofluorescence, and then washed in 70% ethanol for 1 min, followed by an additional wash in PBS. Nuclei were counterstained with Hoechst 33528 or DAPI, and coverslips were mounted in Mowiol (Sigma-Aldrich) or mounting medium (DakoCytomation). Sections were imaged on a confocal microscope (Zeiss LSM 880 or Leica TCS SPE).

#### 4.9 | SA- $\beta$ -Galactosidase activity

The SA- $\beta$ -Galactosidase (SA- $\beta$ -Gal) activity was performed with the SA- $\beta$ -Gal staining kit (Cell Signaling) according to the manufacturer's instructions. Briefly, control and senescent astrocyte cultures were incubated with the fixative solution at RT for 15 min, washed with PBS, and incubated with the  $\beta$ -galactosidase staining solution at 37°C in a dry incubator overnight. Subsequently, the SA- $\beta$ -Gal staining was quantified under a TE2000 Nikon microscope. The optical density of the X-Gal color was determined with the Threshold color plugin from Image J software (NIH), which converts the blue

color to grayscale. The optical density of each field was normalized by the number of cells labeled by DAPI. This method of quantifying chromogen-developed images has been previously described (Figueiredo et al., 2013). Complementarily, the number of  $\beta$ -Gal positive cells was quantified and normalized by the number of cells labeled by DAPI per field.

#### 4.10 | Reactive oxygen species measurement

Dihydroethidium (DHE; Invitrogen) was freshly prepared before each experiment. Control and senescent astrocytes cultures were loaded with DHE at a final concentration of 10  $\mu$ M for 40 min, and cells were immediately imaged on a TE2000 Nikon microscope. DHE intensity was quantified using ImageJ software as previously described (Diniz et al., 2017).

#### 4.11 | Nitrite measurement

NO production was determined indirectly through the assay of nitrite (NO<sub>2</sub>), a stable metabolite of NO, according to the Griess reaction (Ding et al., 1998). Briefly, a 50  $\mu$ l aliquot of control or senescent ACM was mixed with an equal volume of Griess reagent (0.1% N-[1-naphthyl] ethylenediamine dihydrochloride, 1% sulfanilamide, and 2.5% phosphoric acid) and incubated at 22°C for 10 min, followed by the absorbance measurement at 540 nm. Based on a standard curve of NaNO<sub>2</sub> (Sigma-Aldrich) ranging from 0 to 100  $\mu$ M, nitrite concentration was calculated. Background NO<sub>2</sub><sup>-</sup> was subtracted from each experimental value.

#### 4.12 | Quantitative RT-PCR

The cortical astrocytes were lysed with TRIzol® (Invitrogen), and total RNA was isolated and purified with Direct-zol™ MiniPrep Plus (Zymo Research) according to the manufacturer's protocol. The RNA was quantified using a NanoDrop ND-1000 spectrophotometer (Thermo Fisher Scientific). The total RNA (1–2  $\mu$ g) was reverse transcribed with a GoScript™ Reverse Transcriptase cDNA reverse transcription kit according to the manufacturer's instructions (Promega Corporation, an affiliate of Promega Biotecnologia do Brasil, Ltda). Primers were designed and synthesized by IDT-DNA. The specific forward and reverse oligonucleotides were as follows: p16<sup>INK4a</sup>: (F) CAG CTC TTC TGC TCA ACT AC, (R) CGC ACG ATG TCT TGA TGT; MMP3: (F) CTG AAG GAG AGG CTG ACA TA, (R) GAG CAG CAA CCA GGA ATA G; IL-1 $\beta$ : (F) CAG GCA GGC AGT ATC ACT CA, (R) TAA TGG GAA CGT CAC ACA CC; IL-6: (F) CAA AGC CAG AGT CCT TCA GAG, (R) TGG TCC TTA GCC ACT CCT TC; Lamin-B1: (F) CAA CTG ACC TCA TCT GGA AGA AC, (R) TGA AGA CTG TGC TTC TCT GAG C and the reference gene RPLP0: (F) CAG GTG TTT GAC AAC GGC AGC ATT, (R) ACT CAG TCT CCA CAG ACA ATG CCA. Quantitative real-time PCR was performed using Fast SYBR Green



Master Mix qPCR Master Mix (Applied Biosystem™); the cycling conditions were 95°C for 20 s, and 40 cycles of 95°C for 1 s, 60°C for 20 s in the Quant Studio 7 Flex System (Applied Biosystem™). The relative expression levels of the genes were calculated using the  $2^{-\Delta\Delta CT}$  method (Livak & Schmittgen, 2001).

#### 4.13 | Western blotting

Protein concentration in cell extracts was measured by the BCA Protein Assay Kit (Cole-Parmer). Forty micrograms protein/lane was electrophoretically separated on a 10% SDS polyacrylamide gel and electrically transferred onto a Hybond-P PVDF transfer membrane (Millipore) for 1.5 h. Membranes were blocked in PBS-milk 5% at RT for 1 h. Next, membranes were incubated in block solution overnight with the following primary antibodies: rabbit anti-lamin-B1 (1:1000; Abcam) and mouse anti-GAPDH (1:1000; Abcam). Membranes were incubated for 1 h with IRDye 680CW goat anti-mouse antibody and IRDye 800CW goat anti-rabbit antibody (LI-COR, 1:20,000) and then scanned and analyzed using Un-Scan-It gel version 6.1 (Silk Scientific).

#### 4.14 | Densitometric and colocalization analysis of mouse tissue

Hippocampal dentate gyrus, comprising the granular cell layer and the molecular layer was imaged on a confocal microscope (Zeiss LSM 880 or Leica TCS SPE). Densitometry for the immunohistochemistry images was performed using integrated density values generated by the Fiji software (NIH) or the mean intensity values generated by the Leica LAS AF software (Leica Microsystems). Colocalization analysis for 53BP1/Hoechst and TGF- $\beta$ 1/GFAP were quantified by the Leica LAS AF software, in which the colocalization rate between these two channels was obtained per image. Conversely, the colocalization rate of 53BP1/Hoechst in GFAP-positive cells was quantified by randomly selecting GFAP-positive cells with good delimitation relative to other astrocytes per image. Densitometric analysis of lamin-B1 and 53BP1 represents the mean of 2 brain tissue sections per mouse, with 2–3 images per section from 4 to 5 animals per experimental group; TGF- $\beta$ 1 data represent the mean of 1 brain tissue section per mouse, with 1–3 images per section from nine animals per experimental group, as indicated in the respective graph and legend.

#### 4.15 | Densitometric analysis of astrocyte cultures

Densitometry for the immunocytochemistry images was performed using integrated density values generated by the ImageJ software (NIH), and normalized by the number of cells per field. At least 10–15 images were acquired from duplicate coverslips per experimental condition. In the graphs where the control is set at 100%, each control culture was paired with its respective senescent culture and

imaged independently from the other cultures. In the other cases where two or more controls with their respective senescent cultures were imaged together, the control was not set at 100%, since this condition enables the quantification of the mean of the controls and their standard error of the mean (SEM). For each result, the exact number of astrocyte cultures per experimental group is indicated in the graph and legend.

#### 4.16 | Synaptic puncta analysis

Synapse analysis was performed as previously described (Diniz et al., 2017). Briefly, neurons were randomly identified and selected if nuclei staining (DAPI staining) were, at least, two diameters away from the neighboring neuronal nucleus. Neuronal cultures were analyzed by immunostaining for the pre- and post-synaptic markers, synaptophysin, and Spinophilin, respectively. The green and red channels were merged and quantified using the Puncta Analyzer plugin from ImageJ software (NIH). A number of 10–35 images were analyzed per experimental condition, and the exact number of neuronal cultures per experimental group is indicated in the graph and legend.

#### 4.17 | Lamin-B1 three-dimensional reconstruction of senescent astrocytes in vitro

After immunostaining for lamin-B1, astrocytes were observed with a super-resolution fluorescence microscopy Zeiss Elyra PS.1 followed by a structured illumination and maximum z-projection process with ZEN 2011 microscope software (Zeiss, Carl Germany). A 3D reconstruction in 3dmod (IMOD software) based on z-stack fluorescence microscopy was performed to classify the types of nuclear deformations observed in each experimental condition. Thus, we established three types of nuclear deformations: invaginated, evaginated, and aberrant nuclei. Invaginated nuclei showed one clear lamin-B1 invagination; evaginated nuclei showed one clear lamin-B1 protrusion from the nuclear lamina; and aberrant nuclei were those with a combination of more than one invagination, evagination, or additional nuclear abnormalities (Figure S2). For nuclear aberration, evagination, and invagination, 38, 32, 34 slices of one z-stack were used, respectively. Regular nuclei showed a circular shape without any nuclear deformations.

#### 4.18 | Nuclear deformations and circularity measurements on astrocyte cultures

Control and senescent astrocyte cultures were immunostained for lamin-B1, counterstained with DAPI, and images were acquired with a TE2000 Nikon microscope with a 63 $\times$  objective. Based on the previous classification of nuclear deformations through super-resolution fluorescence microscopy and 3D reconstruction, we quantified the relative number of nuclear deformations based on the total number of lamin-B1+ nuclei per image. A total of 3084 cells from nine control



astrocyte cultures and 4481 cells from 10 senescent astrocyte cultures were analyzed. We also calculated the nuclear circularity per lamin-B1+ nuclei using the Fiji software and by employing the formula:  $\text{circularity} = 4\pi (\text{area}/\text{perimeter}^2)$ . Circularity has a maximum value of 1 and diminishes as the nuclear shape becomes increasingly convoluted (Zhang et al., 2018). A total of 1231 and 944 lamin-B1+ nuclei, respectively, were analyzed from 7 and 6, control and senescent astrocyte cultures. Astrocytes cultures were prepared from different litters.

#### 4.19 | Densitometric analysis of human paraffin-embedded tissue

Human paraffin-embedded hippocampal tissues were immunostained for lamin-B1 and counterstained with Hoechst or DAPI. The granular cell layer and the polymorphic layer of the hippocampal dentate gyrus were imaged on a confocal microscope (Zeiss LSM 880 or Leica TCS SPE), using the same image parameters for middle-aged and elderly groups. Densitometry for the immunohistochemistry images was performed using the values of integrated density and nuclear area generated with the Fiji software (NIH). The integrated density was normalized by the area of lamin-B1 immunostaining. The values represent the mean of 2–4 independent hippocampal tissue sections per donor. For each result, the exact number of donors is indicated in the graph and legend.

#### 4.20 | Nuclear deformations and circularity measurements of human paraffin-embedded tissue

Human paraffin-embedded hippocampal tissues were immunostained for lamin-B1 and GFAP, and counterstained with Hoechst or DAPI. We used the same parameters described above (for astrocyte cultures) to quantify the number of invaginated, evaginated, and aberrant nuclei based on lamin-B1 staining. The relative number of nuclear deformations was expressed based on the total number of lamin-B1+ nuclei per image. Tissue sections were imaged on a confocal microscope (Zeiss LSM 880 or Leica TCS SPE), using the same image parameters for middle-aged and elderly groups. Nuclear circularity was calculated per Hoechst (tissue from the NBB) or DAPI (tissue from the BBBABSG) labeled nuclei and in GFAP+ cells at the granular cell layer and polymorphic layer from middle-aged and elderly donors. The total number of cells and nuclei analyzed for each marker and experimental condition is described in Table S2.

#### 4.21 | Statistical analysis

Statistical analysis was done by Student's *t* test or one-way ANOVA, using GraphPad Prism version 8 (GraphPad Software). *P*-value <0.05 was considered statistically significant. Error bars represent the standard error of the mean (SEM). For each result, the exact number of experiments, animal samples, or human post-mortem

hippocampal tissue donors are indicated in the graph, legend, and the respective "Experimental procedures" section.

#### ACKNOWLEDGMENTS

We thank Marcelo Meloni, Grasiela Ventura, Jacqueline Sluijs, Daniëlle Vonk and Roland van Dijk for technical assistance. This work was supported by grants from Conselho Nacional de Desenvolvimento Científico e Tecnológico (CNPq) (IM, IVD, LSN, FCAG), Coordenação de Aperfeiçoamento de Pessoal de Nível Superior (CAPES) (IM, LPD), Fundação Carlos Chagas Filho de Amparo à Pesquisa do Estado do Rio de Janeiro (FAPERJ) (IVD, FCAG), Fundação de Amparo à Pesquisa do Estado de São Paulo (FAPESP) (REPL, CS, RN, WJF, LTG), U.S. Department of Health & Human Services, National Institute of Health (LTG), ZonMW Memorabel and Alzheimer Nederland (EMH, JM), Departamento de Ciência e Tecnologia, Ministério da Saúde (Decit-MS) (IM, LPD, APBA, GV, FCAG), Fiocruz-MS-Servier Award (FCAG), Instituto Nacional de Neurociência Translacional (INCT-INNT) (FCAG).

#### CONFLICT OF INTEREST

The authors declare no conflict of interest.

#### AUTHOR CONTRIBUTIONS

IM, EMH, and FCAG: Conceptualization. IM, LPD, IVD, EMH, JM, and FCAG: Research design. IM, LPD, IVD, LSN, APBA, and GV: Research performance. IM, LPD, IVD, LSN, APBA, and GV: Data analysis. EMH, JM, and FCAG: Supervision. IM: Writing-original draft preparation. IM and FCAG: Reviewing and editing. REPL, CKS, RN, WJF, and LTG: Data analysis and resources. EMH, JM, and FCAG: Funding acquisition and project administration.

#### DATA AVAILABILITY STATEMENT

The data that support the findings of this study are available from the corresponding author upon reasonable request.

#### ORCID

Isadora Matias  <https://orcid.org/0000-0002-4421-4487>

Flávia Carvalho Alcantara Gomes  <https://orcid.org/0000-0003-2966-0638>

#### REFERENCES

- Baldwin, K. T., & Eroglu, C. (2017). Molecular mechanisms of astrocyte-induced synaptogenesis. *Current Opinion in Neurobiology*, 45, 113–120. <https://doi.org/10.1016/j.conb.2017.05.006>
- Barbar, L., Jain, T., Zimmer, M., Kruglikov, I., Sadick, J. S., Wang, M., Kalpana, K., Rose, I. V. L., Burstein, S. R., Rusielewicz, T., Nijssure, M., Guttenplan, K. A., di Domenico, A., Croft, G., Zhang, B., Nobuta, H., Hébert, J. M., Liddel, S. A., & Fossati, V. (2020). CD49f is a novel marker of functional and reactive human iPSC-derived astrocytes. *Neuron*, 107(3), 436–453.e12. <https://doi.org/10.1016/j.neuron.2020.05.014>
- Bedrosian, T. A., Houtman, J., Eguiguren, J. S., Ghassemzadeh, S., Rund, N., Novaresi, N. M., Hu, L., Parylak, S. L., Denli, A. M., Randolph-Moore, L., Namba, T., Gage, F. H., & Toda, T. (2020). Lamin B1 decline underlies age-related loss of adult hippocampal neurogenesis. *EMBO*



- Journal*, 40(3), e105819. <https://doi.org/10.15252/embj.2020105819>
- Bellaver, B., Souza, D. G., Souza, D. O., & Quincozes-Santos, A. (2017). Hippocampal astrocyte cultures from adult and aged rats reproduce changes in glial functionality observed in the aging brain. *Molecular Neurobiology*, 54, 2969–2985 <https://doi.org/10.1007/s12035-016-9880-8>
- Bhat, R., Crowe, E. P., Bitto, A., Moh, M., Katsetos, C. D., Garcia, F. U., Johnson, F. B., Trojanowski, J. Q., Sell, C., & Torres, C. (2012). Astrocyte senescence as a component of Alzheimer's disease. *PLoS One*, 7, e45069 <https://doi.org/10.1371/journal.pone.0045069>
- Bigagli, E., Luceri, C., Scartabelli, T., Dolara, P., Casamenti, F., Pellegrini-Giampietro, D. E., & Giovannelli, L. (2016). Long-term neuroglial cocultures as a brain aging model: Hallmarks of senescence, miRNA expression profiles, and comparison with in vivo models. *The Journals of Gerontology. Series A, Biological Sciences and Medical Sciences*, 71, 50–60 <https://doi.org/10.1093/geron/glu231>
- bin Imtiaz, M. K., Jaeger, B. N., Bottes, S., Machado, R. A. C., Vidmar, M., Moore, D. L., & Jessberger, S. (2021). Declining lamin B1 expression mediates age-dependent decreases of hippocampal stem cell activity. *Cell Stem Cell*, 28, 967–977.e8 <https://doi.org/10.1016/j.stem.2021.01.015>
- Boisvert, M. M., Erikson, G. A., Shokhiev, M. N., & Allen, N. J. (2018). The aging astrocyte transcriptome from multiple regions of the mouse brain. *Cell Reports*, 22, 269–285 <https://doi.org/10.1016/j.celrep.2017.12.039>
- Bussian, T. J., Aziz, A., Meyer, C. F., Swenson, B. L., van Deursen, J. M., & Baker, D. J. (2018). Clearance of senescent glial cells prevents tau-dependent pathology and cognitive decline. *Nature*, 562, 578–582 <https://doi.org/10.1038/s41586-018-0543-y>
- Campisi, J. (2005). Senescent cells, tumor suppression, and organismal aging: Good citizens, bad neighbors. *Cell*, 120, 513–522 <https://doi.org/10.1016/j.cell.2005.02.003>
- Casse, F., Richetin, K., & Toni, N. (2018). Astrocytes' contribution to adult neurogenesis in physiology and Alzheimer's disease. *Frontiers in Cellular Neuroscience*, 12, 432 <https://doi.org/10.3389/fncel.2018.00432>
- Chinta, S. J., Woods, G., Demaria, M., Rane, A., Zou, Y., McQuade, A., Rajagopalan, S., Limbad, C., Madden, D. T., Campisi, J., & Andersen, J. K. (2018). Cellular senescence is induced by the environmental neurotoxin paraquat and contributes to neuropathology linked to Parkinson's disease. *Cell Reports*, 22, 930–940. <https://doi.org/10.1016/j.celrep.2017.12.092>
- Clarke, L. E., Liddelow, S. A., Chakraborty, C., Munch, A. E., Heiman, M., & Barres, B. A. (2018). Normal aging induces A1-like astrocyte reactivity. *Proceedings of the National Academy of Sciences of the United States of America*, 115, E1896–E1905 <https://doi.org/10.1073/pnas.1800165115>
- Cohen, J., & Torres, C. (2019). Astrocyte senescence: Evidence and significance. *Aging Cell*, 18, e12937 <https://doi.org/10.1111/accel.12937>
- Coppé, J.-P., Desprez, P.-Y., Krtolica, A., & Campisi, J. (2010). The senescence-associated secretory phenotype: The dark side of tumor suppression. *Annual Review of Pathology: Mechanisms of Disease*, 5, 99–118 <https://doi.org/10.1146/annurev-pathol-121808-102144>
- de Leeuw, R., Gruenbaum, Y., & Medalia, O. (2018). Nuclear lamins: Thin filaments with major functions. *Trends in Cell Biology*, 28, 34–45 <https://doi.org/10.1016/j.tcb.2017.08.004>
- Di Micco, R., Krizhanovsky, V., Baker, D., & d'Adda di Fagagna, F. (2021). Cellular senescence in ageing: From mechanisms to therapeutic opportunities. *Nature Reviews Molecular Cell Biology*, 22, 75–95 <https://doi.org/10.1038/s41580-020-00314-w>
- Ding, M., Zhang, M., Wong, J. L., Rogers, N. E., Ignarro, L. J., & Voskuhl, R. R. (1998). Antisense knockdown of inducible nitric oxide synthase inhibits induction of experimental autoimmune encephalomyelitis in SJL/J mice. *The Journal of Immunology*, 160, 2560–2564
- Diniz, L. P., Matias, I., Araujo, A. P. B., Garcia, M. N., Barros-Aragão, F. G. Q., Alves-Leon, S. V., de Souza, J. M., Foguel, D., Figueiredo, C. P., Braga, C., Romão, L., & Gomes, F. C. A. (2019).  $\alpha$ -synuclein oligomers enhance astrocyte-induced synapse formation through TGF- $\beta$ 1 signaling in a Parkinson's disease model. *Journal of Neurochemistry*, 150, 138–157 <https://doi.org/10.1111/jnc.14710>
- Diniz, L. P., Tortelli, V., Matias, I., Morgado, J., Bergamo Araujo, A. P., Melo, H. M., Seixas da Silva, G. S., Alves-Leon, S. V., de Souza, J. M., Ferreira, S. T., De Felice, F. G., & Gomes, F. C. A. (2017). Astrocyte transforming growth factor beta 1 protects synapses against abeta oligomers in Alzheimer's disease model. *The Journal of Neuroscience*, 37, 6797–6809
- Figueiredo, C. P., Clarke, J. R., Ledo, J. H., Ribeiro, F. C., Costa, C. V., Melo, H. M., Mota-Sales, A. P., Saraiva, L. M., Klein, W. L., Sebollela, A., De Felice, F. G., & Ferreira, S. T. (2013). Memantine rescues transient cognitive impairment caused by high-molecular-weight A oligomers but not the persistent impairment induced by low-molecular-weight oligomers. *Journal of Neuroscience*, 33, 9626–9634
- Freund, A., Laberge, R. M., Demaria, M., & Campisi, J. (2012). Lamin B1 loss is a senescence-associated biomarker. *Molecular Biology of the Cell*, 23, 2066–2075. <https://doi.org/10.1091/mbc.e11-10-0884>
- Frost, B., Bardai, F. H., & Feany, M. B. (2016). Lamin dysfunction mediates neurodegeneration in tauopathies. *Current Biology*, 26, 129–136
- Fu, H., Hardy, J., & Duff, K. E. (2018). Selective vulnerability in neurodegenerative diseases. *Nature Neuroscience*, 21, 1350–1358 <https://doi.org/10.1038/s41593-018-0221-2>
- Guo, Y., Kim, Y., Shimi, T., Goldman, R. D., & Zheng, Y. (2014). Concentration-dependent lamin assembly and its roles in the localization of other nuclear proteins. *MBoC*, 25, 1287–1297 <https://doi.org/10.1091/mbc.e13-11-0644>
- Herbig, U., Ferreira, M., Condel, L., Carey, D., & Sedivy, J. M. (2006). Cellular senescence in aging primates. *Science*, 311, 1257 <https://doi.org/10.1126/science.1122446>
- Ho, C. Y., & Lammerding, J. (2012). Lamins at a glance. *Journal of Cell Science*, 125, 2087–2093 <https://doi.org/10.1242/jcs.087288>
- Hou, Y., Dan, X., Babbar, M., Wei, Y., Hasselbalch, S. G., Croteau, D. L., & Bohr, V. A. (2019). Ageing as a risk factor for neurodegenerative disease. *Nature Reviews Neurology*, 15, 565–581 <https://doi.org/10.1038/s41582-019-0244-7>
- Kawano, H., Katsurabayashi, S., Kakazu, Y., Yamashita, Y., Kubo, N., Kubo, M., Okuda, H., Takasaki, K., Kubota, K., Mishima, K., Fujiwara, M., Harata, N. C., & Iwasaki, K. (2012). Long-term culture of astrocytes attenuates the readily releasable pool of synaptic vesicles. *PLoS One*, 7, e48034 <https://doi.org/10.1371/journal.pone.0048034>
- Limbad, C., Oron, T. R., Alimirah, F., Davalos, A. R., Tracy, T. E., Gan, L., Desprez, P.-Y., & Campisi, J. (2020). Astrocyte senescence promotes glutamate toxicity in cortical neurons. *PLoS One*, 15, e0227887. <https://doi.org/10.1371/journal.pone.0227887>
- Livak, K. J., & Schmittgen, T. D. (2001). Analysis of relative gene expression data using real-time quantitative PCR and the 2(-Delta Delta C(T)) Method. *Methods*, 25, 402–408
- Lopez-Otin, C., Blasco, M. A., Partridge, L., Serrano, M., & Kroemer, G. (2013). The hallmarks of aging. *Cell*, 153, 1194–1217 <https://doi.org/10.1016/j.cell.2013.05.039>
- Martínez-Cué, C., & Rueda, N. (2020) Cellular senescence in neurodegenerative diseases. *Frontiers in Cellular Neuroscience*, 14, <https://doi.org/10.3389/fncel.2020.00016>
- Matias, I., Diniz, L. P., Buosi, A., Neves, G., Stipursky, J., & Gomes, F. C. A. (2017). Flavonoid hesperidin induces synapse formation and improves memory performance through the astrocytic TGF-beta1. *Frontiers in Aging Neuroscience*, 9, 184





- Matias, I., Morgado, J., & Gomes, F. C. A. (2019). Astrocyte heterogeneity: Impact to brain aging and disease. *Frontiers in Aging Neuroscience*, 11, 59. <https://doi.org/10.3389/fnagi.2019.00059>
- Mehta, I. S., Figgitt, M., Clements, C. S., Kill, I. R., & Bridger, J. M. (2007). Alterations to nuclear architecture and genome behavior in senescent cells. *Annals of the New York Academy of Sciences*, 1100, 250–263
- Morrison, J. H., & Baxter, M. G. (2012). The ageing cortical synapse: Hallmarks and implications for cognitive decline. *Nature Reviews. Neuroscience*, 13, 240–250
- Munoz-Espin, D., & Serrano, M. (2014). Cellular senescence: From physiology to pathology. *Nature Reviews. Molecular Cell Biology*, 15, 482–496
- Nadal, L., Coupé, P., Helmer, C., Manjon, J. V., Amieva, H., Tison, F., Dartigues, J.-F., Catheline, G., & Planche, V. (2020). Differential annualized rates of hippocampal subfields atrophy in aging and future Alzheimer's clinical syndrome. *Neurobiology of Aging*, 90, 75–83 <https://doi.org/10.1016/j.neurobiolaging.2020.01.011>
- Nations U (2017). World population ageing 2015. Available at: <https://www.un-ilibrary.org/content/publication/88fa44e7-en>
- Oberheim, N. A., Takano, T., Han, X., He, W., Lin, J. H., Wang, F., Xu, Q., Wyatt, J. D., Pilcher, W., Ojemann, J. G., Ransom, B. R., Goldman, S. A., & Nedergaard, M. (2009). Uniquely hominid features of adult human astrocytes. *The Journal of Neuroscience*, 29, 3276–3287 <https://doi.org/10.1523/JNEUROSCI.4707-08.2009>
- Orre, M., Kamphuis, W., Osborn, L. M., Melief, J., Kooijman, L., Huitinga, I., Klooster, J., Bossers, K., & Hol, E. M. (2014). Acute isolation and transcriptome characterization of cortical astrocytes and microglia from young and aged mice. *Neurobiology of Aging*, 35, 1–14 <https://doi.org/10.1016/j.neurobiolaging.2013.07.008>
- Osborn, L. M., Kamphuis, W., Wadman, W. J., & Hol, E. M. (2016). Astroglia: An integral player in the pathogenesis of Alzheimer's disease. *Progress in Neurobiology*, 144, 121–141. <https://doi.org/10.1016/j.pneurobio.2016.01.001>
- Paonessa, F., Evans, L. D., Solanki, R., Larriue, D., Wray, S., Hardy, J., Jackson, S. P., & Livesey, F. J. (2019). Microtubules deform the nuclear membrane and disrupt nucleocytoplasmic transport in tau-mediated frontotemporal dementia. *Cell Reports*, 26, 582–593.e5 <https://doi.org/10.1016/j.celrep.2018.12.085>
- Pertusa, M., Garcia-Matas, S., Rodriguez-Farre, E., Sanfeliu, C., & Cristofol, R. (2007). Astrocytes aged in vitro show a decreased neuroprotective capacity. *Journal of Neurochemistry*, 101, 794–805. <https://doi.org/10.1111/j.1471-4159.2006.04369.x>
- Pestana, F., Edwards-Faret, G., Belgard, T. G., Martirosyan, A., & Holt, M. G. (2020) No longer underappreciated: The emerging concept of astrocyte heterogeneity in neuroscience. *Brain Sciences*, 10(3), 168.
- Roussarie, J.-P., Yao, V., Rodriguez-Rodriguez, P., Oughtred, R., Rust, J., Plautz, Z., Kasturia, S., Albornoz, C., Wang, W., Schmidt, E. F., Dannenfels, R., Tadych, A., Brichta, L., Barnea-Cramer, A., Heintz, N., Hof, P. R., Heiman, M., Dolinski, K., Flajolet, M., ... Greengard, P. (2020). Selective neuronal vulnerability in Alzheimer's disease: A network-based analysis. *Neuron*, 107(5), 821–835.E12.
- Saito, N., Araya, J., Ito, S., Tsubouchi, K., Minagawa, S., Hara, H., Ito, A., Nakano, T., Hosaka, Y., Ichikawa, A., Kadota, T., Yoshida, M., Fujita, Y., Utsumi, H., Kurita, Y., Kobayashi, K., Hashimoto, M., Wakui, H., Numata, T., ... Kuwano, K. (2019). Involvement of lamin B1 reduction in accelerated cellular senescence during chronic obstructive pulmonary disease pathogenesis. *The Journal of Immunology*, 202, 1428–1440. <https://doi.org/10.4049/jimmunol.1801293>
- Salminen, A., Ojala, J., Kaarniranta, K., Haapasalo, A., Hiltunen, M., & Soininen, H. (2011). Astrocytes in the aging brain express characteristics of senescence-associated secretory phenotype. *The European Journal of Neuroscience*, 34, 3–11. <https://doi.org/10.1111/j.1460-9568.2011.07738.x>
- Schaum, N., Lehallier, B., Hahn, O., Pálovics, R., Hosseinzadeh, S., Lee, S. E., Sit, R., Lee, D. P., Losada, P. M., Zardeneta, M. E., Fehlmann, T., Webber, J. T., McGeever, A., Calcuttawala, K., Zhang, H., Berdnik, D., Mathur, V., Tan, W., Zee, A., ... Wyss-Coray, T. (2020). Ageing hallmarks exhibit organ-specific temporal signatures. *Nature*, 583, 596–602. <https://doi.org/10.1038/s41586-020-2499-y>
- Schreiber, K. H., & Kennedy, B. K. (2013). When lamins go bad: Nuclear structure and disease. *Cell*, 152, 1365–1375. <https://doi.org/10.1016/j.cell.2013.02.015>
- Shang, D., Hong, Y., Xie, W., Tu, Z., & Xu, J. (2020). Interleukin-1 $\beta$  drives cellular senescence of rat astrocytes induced by oligomerized amyloid  $\beta$  peptide and oxidative stress. *Frontiers in Neurology*, 11, 929. <https://doi.org/10.3389/fneur.2020.00929>
- Sharpless, N. E., & Sherr, C. J. (2015). Forging a signature of in vivo senescence. *Nature Reviews. Cancer*, 15, 397–408.
- Shimi, T., Butin-Israeli, V., Adam, S. A., Hamanaka, R. B., Goldman, A. E., Lucas, C. A., Shumaker, D. K., Kosak, S. T., Chandel, N. S., & Goldman, R. D. (2011). The role of nuclear lamin B1 in cell proliferation and senescence. *Genes & Development*, 25, 2579–2593. <https://doi.org/10.1101/gad.179515.111>
- Small, S. A., Schobel, S. A., Buxton, R. B., Witter, M. P., & Barnes, C. A. (2011). A pathological framework of hippocampal dysfunction in ageing and disease. *Nature Reviews. Neuroscience*, 12, 585–601
- Soreq, L., Rose, J., Soreq, E., Hardy, J., Trabzuni, D., Cookson, M. R., Smith, C., Ryten, M., Patani, R., & Ule, J. (2017). Major shifts in glial regional identity are a transcriptional hallmark of human brain aging. *Cell Reports*, 18, 557–570. <https://doi.org/10.1016/j.celrep.2016.12.011>
- Souza, D. G., Bellaver, B., Raupp, G. S., Souza, D. O., & Quincozes-Santos, A. (2015). Astrocytes from adult Wistar rats aged in vitro show changes in glial functions. *Neurochemistry International*, 90, 93–97
- Tominaga, K., & Suzuki, H. I. (2019). TGF- $\beta$  signaling in cellular senescence and aging-related pathology. *International Journal of Molecular Sciences*, 20, 5002. <https://doi.org/10.3390/ijms20205002>
- Turnquist, C., Beck, J. A., Horikawa, I., Obiorah, I. E., Von Muhlinen, N., Vojtesek, B., Lane, D. P., Grunseich, C., Chahine, J. J., Ames, H. M., Smart, D. D., Harris, B. T., & Harris, C. C. (2019). Radiation-induced astrocyte senescence is rescued by  $\Delta 133p53$ . *Neuro-Oncology*, 21, 474–485 <https://doi.org/10.1093/neuonc/noz001>
- van Strien, M. E., Sluijs, J. A., Reynolds, B. A., Steindler, D. A., Aronica, E., & Hol, E. M. (2014). Isolation of neural progenitor cells from the human adult subventricular zone based on expression of the cell surface marker CD271. *Stem Cells Translational Medicine*, 3, 470–480. <https://doi.org/10.5966/sctm.2013-0038>
- Verkhratsky, A., & Nedergaard, M. (2018). Physiology of astroglia. *Physiological Reviews*, 98, 239–389.
- Wang, A. S., Ong, P. F., Chojnowski, A., Clavel, C., & Dreesen, O. (2017). Loss of lamin B1 is a biomarker to quantify cellular senescence in photoaged skin. *Scientific Reports*, 7, 15678. <https://doi.org/10.1038/s41598-017-15901-9>
- Wang, C., Jurk, D., Maddick, M., Nelson, G., Martin-Ruiz, C., & von Zglinicki, T. (2009). DNA damage response and cellular senescence in tissues of aging mice. *Aging Cell*, 8, 311–323. <https://doi.org/10.1111/j.1474-9726.2009.00481.x>
- Yousefzadeh, M. J., Zhao, J., Bukata, C., Wade, E. A., McGowan, S. J., Angelini, L. A., Bank, M. P., Gurkar, A. U., McGuckian, C. A., Calubag, M. F., Kato, J. I., Burd, C. E., Robbins, P. D., & Niedernhofer, L. J. (2020). Tissue specificity of senescent cell accumulation during physiologic and accelerated aging of mice. *Aging Cell*, 19, e13094. <https://doi.org/10.1111/accel.13094>
- Yue, S., Zheng, X., & Zheng, Y. (2019). Cell-type-specific role of lamin-B1 in thymus development and its inflammation-driven reduction in thymus aging. *Aging Cell*, 18, e12952. <https://doi.org/10.1111/accel.12952>



- Zhang, P., Kishimoto, Y., Grammatikakis, I., Gottimukkala, K., Cutler, R. G., Zhang, S., Abdelmohsen, K., Bohr, V. A., Misra Sen, J., Gorospe, M., & Mattson, M. P. (2019). Senolytic therapy alleviates A $\beta$ -associated oligodendrocyte progenitor cell senescence and cognitive deficits in an Alzheimer's disease model. *Nature Neuroscience*, 22, 719–728.
- Zhang, Y., Wang, J., Huang, W., Cai, J., Ba, J., Wang, Y., Ke, Q., Huang, Y., Liu, X., Qiu, Y., Lu, Q., Sui, X., Shi, Y., Wang, T., Shen, H., Guan, Y., Zhou, Y., Chen, Y., Wang, M., & Xiang, A. P. (2018). Nuclear Nestin deficiency drives tumor senescence via lamin A/C-dependent nuclear deformation. *Nature Communications*, 9, 3613. <https://doi.org/10.1038/s41467-018-05808-y>

**How to cite this article:** Matias, I., Diniz, L. P., Damico, I. V., Araujo, A. P. B., Neves, L. D. S., Vargas, G., Leite, R. E. P., Suemoto, C. K., Nitrini, R., Jacob-Filho, W., Grinberg, L. T., Hol, E. M., Middeldorp, J., & Gomes, F. C. A. (2022). Loss of lamin-B1 and defective nuclear morphology are hallmarks of astrocyte senescence in vitro and in the aging human hippocampus. *Aging Cell*, 21, e13521. <https://doi.org/10.1111/ace1.13521>

## SUPPORTING INFORMATION

Additional supporting information may be found in the online version of the article at the publisher's website.